

Award Number: W81XWH-11-1-0330

TITLE: Translational Research for Muscular Dystrophy

PRINCIPAL INVESTIGATOR: Gregory A. Cox, Ph.D.

CONTRACTING ORGANIZATION: The Jackson Laboratory
Bar Harbor, ME 04609

REPORT DATE: July 2015

TYPE OF REPORT: Final

PREPARED FOR: U.S. Army Medical Research and Materiel Command
Fort Detrick, Maryland 21702-5012

DISTRIBUTION STATEMENT: Approved for Public Release;
Distribution Unlimited

The views, opinions and/or findings contained in this report are those of the author(s) and should not be construed as an official Department of the Army position, policy or decision unless so designated by other documentation.

REPORT DOCUMENTATION PAGE				Form Approved OMB No. 0704-0188	
Public reporting burden for this collection of information is estimated to average 1 hour per response, including the time for reviewing instructions, searching existing data sources, gathering and maintaining the data needed, and completing and reviewing this collection of information. Send comments regarding this burden estimate or any other aspect of this collection of information, including suggestions for reducing this burden to Department of Defense, Washington Headquarters Services, Directorate for Information Operations and Reports (0704-0188), 1215 Jefferson Davis Highway, Suite 1204, Arlington, VA 22202-4302. Respondents should be aware that notwithstanding any other provision of law, no person shall be subject to any penalty for failing to comply with a collection of information if it does not display a currently valid OMB control number. PLEASE DO NOT RETURN YOUR FORM TO THE ABOVE ADDRESS.					
1. REPORT DATE July 2015		2. REPORT TYPE Final		3. DATES COVERED 05/01/2011 - 04/30/2015	
4. TITLE AND SUBTITLE Translational Research for Muscular Dystrophy				5a. CONTRACT NUMBER	
				5b. GRANT NUMBER W81XWH-11-1-0330	
				5c. PROGRAM ELEMENT NUMBER	
6. AUTHOR(S) Gregory A. Cox, Ph.D. E-Mail: greg.cox@jax.org				5d. PROJECT NUMBER	
				5e. TASK NUMBER	
				5f. WORK UNIT NUMBER	
7. PERFORMING ORGANIZATION NAME(S) AND ADDRESS(ES) The Jackson Laboratory 600 Main Street Bar Harbor, ME 04609-1523				8. PERFORMING ORGANIZATION REPORT NUMBER	
9. SPONSORING / MONITORING AGENCY NAME(S) AND ADDRESS(ES) U.S. Army Medical Research and Materiel Command Fort Detrick, Maryland 21702-5012				10. SPONSOR/MONITOR'S ACRONYM(S)	
				11. SPONSOR/MONITOR'S REPORT NUMBER(S)	
12. DISTRIBUTION / AVAILABILITY STATEMENT Approved for Public Release; Distribution Unlimited					
13. SUPPLEMENTARY NOTES					
14. ABSTRACT The overall goal of this work is to increase the availability of critical mouse models of human muscular dystrophy (MD) for both hypothesis testing and preclinical therapy development. Our multi-disciplinary team from The Jackson Laboratory (JAX) and the Children's National Medical Center (CNMC) has expertise in MD, repository management, mouse models, and preclinical testing. Over the course of this funding, Drs. Lutz and Cox at JAX have added 15 new strains to the MD Repository (Aim1) to leverage JAX's considerable expertise and infrastructure to maintain and distribute MD mouse resources to the scientific community. In Aim 2 we have completed gene targeting of dystrophin transgenes into DBA/2J ES cell lines and have achieved germ-line transmission from each line. These novel DMD transgenic mice, which model patients receiving successful exon-skipping therapies, will be crossed to mutant D2.B10-mdx to score for phenotypic rescue of each mutant and WT line to compare the functionality of resulting dystrophin molecules containing in-frame deletions that are expected to arise by successful treatment of patient mutations. In Aim 3, we have completed generation of a DBA/2J congenic mdx strain that appears to better model the symptoms of the human disease. Moving the mdx mutation onto different genetic backgrounds has shown the power of genetic variation among inbred strains to alter the disease onset and progression in order to improve the pre-clinical efficacy. In Aim 4, Dr. Nagaraju at CNMC has performed a baseline phenotypic analysis of our new D2.B10-mdx model and we have combined the analysis from JAX and CNMC into a manuscript, currently under revision at Human Molecular Genetics, detailing the advantages of this new model for preclinical testing. Our DMD repository has greatly expand the accessibility and availability of mouse model resources for MD translational research and therapeutic development.					
15. SUBJECT TERMS Nothing Listed					
16. SECURITY CLASSIFICATION OF:			17. LIMITATION OF ABSTRACT	18. NUMBER OF PAGES	19a. NAME OF RESPONSIBLE PERSON
a. REPORT	b. ABSTRACT	c. THIS PAGE			USAMRMC
U	U	U	UU	62	19b. TELEPHONE NUMBER (include area code)

Table of Contents

	<u>Page</u>
Introduction.....	4
Body.....	4
Key Research Accomplishments.....	10
Reportable Outcomes.....	11
Conclusion.....	12
Appendices.....	13

A. INTRODUCTION

The goal of this work is to increase the availability of critical mouse models of human muscular dystrophy (MD) for both hypothesis testing and preclinical therapy development. Our multi-disciplinary team from The Jackson Laboratory (JAX) and the Children's National Medical Center (CNMC) has expertise in MD, repository management, mouse models, and preclinical testing. At JAX, Drs. Lutz and Cox have established the MD Repository (Aim1) to leverage JAX's considerable expertise and infrastructure to maintain and distribute MD mouse and information resources to the scientific community. In Aim 2 we have developed novel DMD transgenic mice, which model patients receiving successful exon-skipping therapies. We propose to address the fundamental, but often overlooked question related to the functionality of resulting Dystrophin molecules containing in-frame deletions that are expected to arise by successful treatment of patient mutations. Our transgenic experiments will model the best-case-scenario outcome for AO-mediated therapy in which one assumes that a particular compound is capable of 100% effective exon-skipping to restore the reading frame. In Aim 3, we have generated congenic *mdx* mice to better model the symptoms of the human disease and to identify genetic modifiers that can alter disease onset and severity. In Aim 4, Dr. Nagaraju at CNMC has carried out preclinical studies with promising therapeutic compounds initially in the C57BL10-*Dmd*^{mdx} but has transitioned to direct phenotypic comparison of the D2.B10-*Dmd*^{mdx} mice so that future drug studies can be completed in this new model developed at JAX. Overall, this program has greatly expanded the accessibility and availability of mouse model resources for MD translational research and therapeutic development.

B. BODY

Aim 1. Develop a centralized repository for mouse models of MD. JAX.

Our goal is to identify, import, and cryopreserve 3-5 biomedically significant models per year for the MD Repository and to disseminate mouse information resources to the scientific community. The repository is providing researchers with centralized access to high-priority DMD models imported from outside investigators and transgenic and congenic DMD models developed in **Aims 2 & 3**. The following lines have been identified as relevant models to the MD Repository at JAX. We have reached out to the investigators who engineered the mice, requesting that they deposit the models to the JAX MD Repository. A description of the successfully imported models is provided below:

1. JAX stock 16587: B6;129-Itga7^{tm1Burk/J}.
Homozygous mice exhibit myopathy, vascular smooth muscle defects, altered extracellular matrix deposition, and altered expression of other integrin chains in the cerebral vasculature.
2. JAX stock 17929: B10.Cg-Cmah^{tm1Avrk} *Dmd*^{mdx}/PtmJ
Compared to homozygous *mdx* mice (*Dmd*^{mdx/mdx} females / *Dmd*^{mdx/Y} males), Cmah-deficiency in homozygous Cmah-*mdx* mice (Cmah^{-/-}; *Dmd*^{mdx/mdx} females / Cmah^{-/-}; *Dmd*^{mdx/Y} males) results in accelerated age of onset, rate of progression, and severity of the major DMD phenotypes contributing to morbidity and mortality. This is especially true for loss of ambulation, cardiac and respiratory muscle weakness, and loss of lifespan.

3. JAX Stock 16622: STOCK *Utrn*^{tm1Jrs} *Dmd*^{mdx}/J
Mice homozygous for the utrophin (*Utrn*^{tm1Jrs}) and *Dmd*^{mdx} alleles have a lifespan of 4 to 20 weeks, with only 50% surviving beyond 8 weeks of age. The double mutants exhibit kyphosis, compromised systolic and diastolic function, progressive fibrosis throughout the heart, cardiomyocyte membrane damage, ventricular cellular necrosis, and disorganized mitochondria and myofibrils in cardiomyocytes.
4. JAX stock 013786: B6.129S1(Cg)-*Lama2*^{tm1Eeng}/J
Homozygous mice exhibit growth retardation and most die between 2-4 weeks of age. Laminin2 is expressed in striated muscle, peripheral and central nervous systems, thymus, thyroid, intestine, and testis and has been associated with merosin-deficient congenital muscular dystrophy (MCMD) .
5. JAX stock 18157: B6.Cg-*Mtm1*^{tm1ltl}/J
These *Mtm1* p.R69C mice contain the p.R69C mutation in exon 4 of the endogenous X-linked myotubular myopathy gene 1 (*Mtm1*) gene. This mutation induces exon skipping of exon 4 and introduces a premature stop codon in exon 5, analogous to an *Mtm1* mutation found in humans with X-linked myotubular myopathy (MTM).
6. JAX stock 18135: C57BL/6-*Cfl2*^{tm1Begg}/J
These *Cofilin2* floxed mutant mice possess *loxP* sites flanking exons 2-4 of the cofilin 2 (*Cfl2*) gene. When these mice are bred to mice that express Cre recombinase, resulting offspring will have exons 2-4 deleted in *cre*-expressing tissues.
7. JAX stock 18284: 129-*Acta1*^{tm1Hrd}/J
The *Acta1*(H40Y) knock-in allele has the endogenous α -skeletal actin sequences replaced by a mutant α -skeletal actin containing the single amino acid change (H40Y) associated with dominantly-inherited severe nemaline myopathy in humans. *Acta1*(H40Y) heterozygotes display clinical and pathological features of patients with nemaline myopathy, including severe, early onset limb and eyelid muscle weakness, decreased mobility, presence of cytoplasmic and nuclear nemaline rods, and increased mortality.
8. JAX stock 18312: FVB/N-Tg(ACTA1-TPM3*M9R)4Hrd/MbngJ
HSA- α Tm_{slow}(Met9Arg) transgenic mice exhibit an overexpression of a dominant-negative alpha-tropomyosin slow Met9Arg mutation associated with human nemaline myopathy (NM) directed to fast-twitch glycolytic skeletal muscle (type 2B) fibers. Transgenic mice display features of NM in skeletal muscle tissue, including electron-dense accumulations (nemaline rods), increased slow/oxidative fiber content, and late-onset skeletal muscle weakness.
9. JAX stock 14563: STOCK *Utrn*^{tm1Ked} *Dmd*^{mdx}/J
Mice that are homozygous for the *Utrn*^{tm1Ked} allele and the *Dmd*^{mdx} allele exhibit a more severe phenotype than single *Dmd*^{mdx} mutants: earlier onset of muscle dystrophy (degeneration, macrophage infiltration and necrosis), weight loss after weaning, joint contractures, kyphosis, dystrophy of extraocular muscles, abnormal electrocardiograms, infertility and premature death.
10. JAX stock 18018: B10ScSn.Cg-*Prkdc*^{scid} *Dmd*^{mdx}/J
When the *Dmd*^{mdx} mutation is combined with the *Prkdc*^{scid} allele, there is some amelioration of the mdx phenotype including a reduction in the rate of muscle fibrosis, higher endurance and decreased expression of active TGFB1. However, MDX/SCID mice continue to exhibit necrosis, centrally located nuclei and the muscle degeneration characteristic of DMD. The MDX/SCID mouse may be used a dystrophic model for the transplantation of human donor cells to evaluate skeletal muscle regeneration.

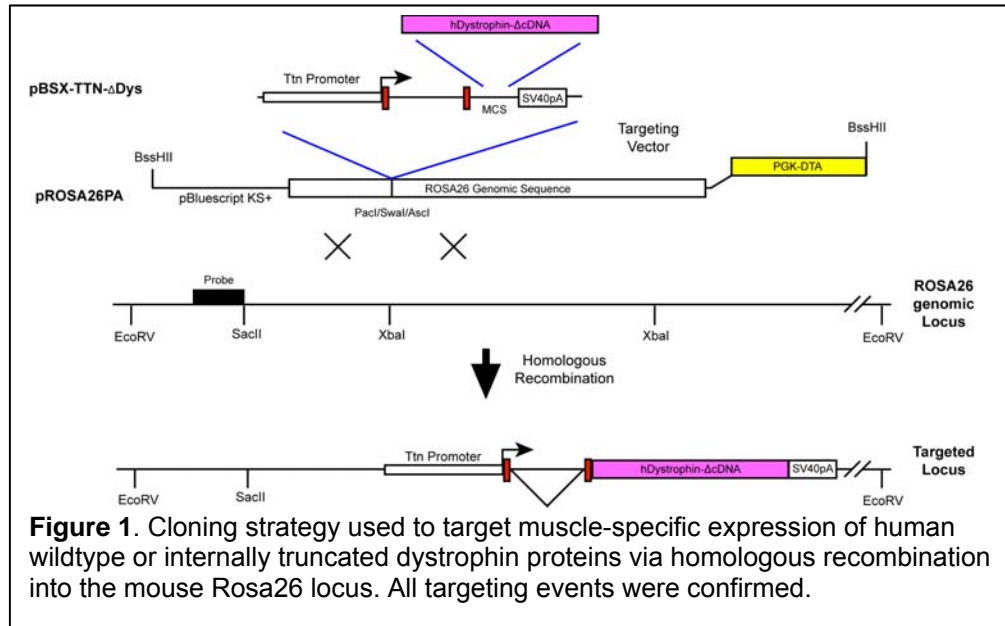
11. JAX stock 13141: D2.B10-*Dmd*^{mdx}/J
The DBA/2-congenic *Dmd*^{mdx} mouse may be a superior Duchenne muscular dystrophy model as it better recapitulates several of the human characteristics of DMD myopathology (lower hind limb muscle weight, fewer myofibers, increased fibrosis and fat accumulation, and muscle weakness).
12. JAX stock 23535: B6.Cg-*Terc*^{tm1Rdp} *Dmd*^{mdx-4Cv}/BlauJ
T *mdx/mTR*^{KO} mouse model combines dystrophin-deficiency with telomere dysfunction/shortening, and may be a superior Duchenne muscular dystrophy model as it better recapitulates several of the human characteristics of DMD myopathology (progressive muscle weakness and damage, skeletal muscle fibrosis, diminished muscle stem cell regenerative capacity, dilated cardiomyopathy, heart failure and shortened life-span).
13. JAX stock 18305: MYD/Le-*Large*^{myd}/J
The spontaneous autosomal recessive mutation myodystrophy (*myd*) is a deletion in exons 5-7 of the glycotransferase gene (*Large*) on chromosome 8; causing a frameshift and premature stop codon before the first two catalytic domains. This *Large*^{myd} mutation results in abnormal glycosylation of its substrate α -dystroglycan. *Large*^{myd} mice are a model of Congenital muscular dystrophy type 1D (MDC1D; also called human α -dystroglycan glycosylation-deficient muscular dystrophy).
14. JAX stock 17917: B6.Cg-*Dysf*^{prmd} *Prkdc*^{scid}/J
These Scid/blAJ mice are a C57BL/6-congenic line that is dysferlin-deficient and also lack B and T lymphocytes. Their attenuated muscle-damaging immune responses result in a dysferlinopathy that is less severe compared to A/J mice naturally carrying the dysferlin mutation. Scid/blAJ mice may be useful for studying limb-girdle muscular dystrophy type 2B (LGMD2B), Miyoshi myopathy, transplantation studies, complement system / membrane attack pathway / membrane attack complex, and how distinct subpopulations of macrophages can promote muscle injury or repair in muscular dystrophy.
15. JAX stock 19097: B6.129-*Fktn*^{tm1Kcam}/J
These mice carry a floxed allele of *Fktn* (fukutin). When crossed with a Cre strain, tissue-specific knockouts of the gene can be generated. Crosses with *Myf5* (myogenic factor 5) and *Ckm* (creatine kinase, muscle) Cre strains generate dystroglycanopathy mice representative of a spectrum of mild to severe patient diseases.

Disseminate MD mouse and information resources to the scientific community through the MD Repository.

All mice that are available from the MD repository at JAX are readily accessed from our public website at JAX. Each strain has its own public datasheet with a description of the mouse, the development of the model, links to genotyping protocols, and animal husbandry information. For example <http://jaxmice.jax.org/strain/013786.html>

Aim 2. Engineer mice expressing in-frame deletions of the human dystrophin cDNA to model patients receiving successful exon-skipping therapies. JAX.

We have successfully generated the three human dystrophin cDNA clones containing in-frame mutations (deletion of exons 44-45, 49-51, 48-53) along with a full-length wildtype cDNA clone. The cDNAs have been fully sequence verified and plasmid vectors containing each clone are prepared. As shown in **Figure 1**, we have successfully cloned dystrophin cDNAs downstream of the mouse Titin



(Ttn) promoter to drive high-level skeletal and cardiac muscle expression of the transgene. The Ttn promoter construct contains the first non-coding exon 1, the entire first intron and the 5' half of exon 2 truncated just upstream of the start codon. We have had great success using this promoter to drive skeletal and cardiac-specific expression of transgenes in the past and expect that a single-copy insertion into the Rosa26 locus should

provide uniform expression between each of the independent lines of mice generated by homologous recombination. The promoter/cDNA construct was completed in step 1, and has been inserted into a Rosa26 vector containing 5' and 3' homology arms for homologous recombination into ES cell lines. To date, we have successfully generated the three human dystrophin cDNA clones containing in-frame mutations (deletion of exons 44-45, 49-51, 48-53) along with a full-length wildtype cDNA clone. Each construct has been successfully targeted into the Rosa26 locus of DBA/2J ES cells. These ES cell lines have been microinjected into host blastocysts and chimeric mice for each construct have gone on to show germline transmission. The mice are being crossed with our newly generated D2.B10-Dmd^{mdx} congenic strain (produced in Aim 3) to evaluate the ability of each construct to rescue all or part of the Duchenne muscular dystrophy phenotype of the mice. Based on our phenotypic analysis of the DBA.B10-Dmd^{mdx} congenic strain (Aim 3 and 4, below) we are confident that generating DMD genetic resources on the DBA/2J genetic background will be the strongest strategy with the largest biomedical relevance to the community.

Aim 3. Develop improved phenotypic *mdx* mouse models using genetic background variation in mice to map and identify genetic modifiers of disease severity. JAX.

3.1. Create a D2.B10-mdx congenic strain of mice on the DBA/2J genetic background.

Based on descriptions that the DMD^{mdx} mouse model had a more severe phenotype when crossed with a DBA mouse strain, we have completed the backcrossing of the mdx mutation onto the DBA/2J background using a speed congenic approach. The JAX DBA/2J substrain was chosen for this backcross as it was used by the Sanger Center for complete genomic sequencing to facilitate identification of genetic modifiers. The genetic quality control employed by the GRS at JAX during the marker-assisted backcross ensures that the resulting mice contain >99.9% of the DBA/2J background across the genome. Markers were chosen for genotyping out of 2,000+ markers in our set, spaced an

average of approximately 1.5 Mb or 0.75cM apart and have been assayed on over 103 JAX® mouse strains, including virtually all of the most commonly used JAX® inbred and wild-derived inbred strains. Intercrosses between D2.B10-+/mdx heterozygous N5 congenic mice are currently being used to generate homozygous mdx/mdx mice on the DBA/2J genetic background followed for phenotypic analysis.

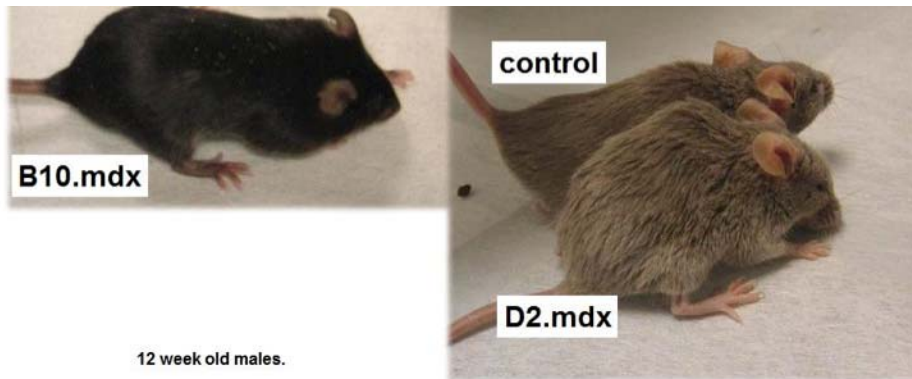


Figure 2. 12 week old males (pictured) show the absence of an overt phenotype in BL10.mdx mice. However, the muscle wasting and kyphosis of the D2.mdx mouse is evident at this early adult age.

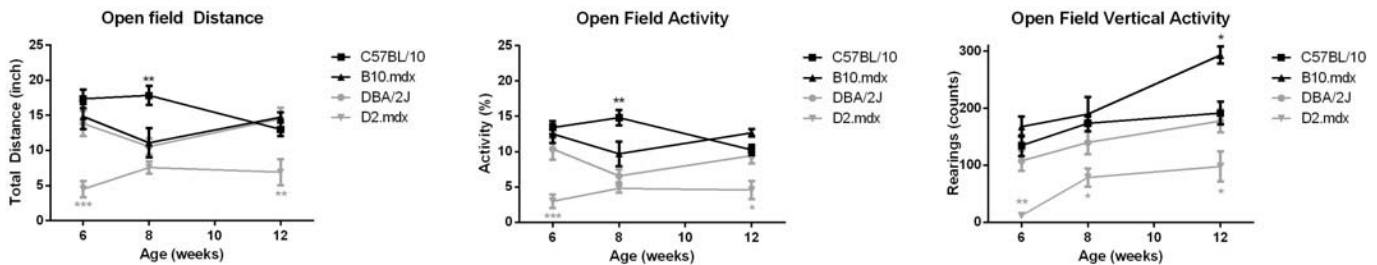


Figure 3. Voluntary locomotor activity, Open Field (n=6-12 /group, males only) demonstrates that the D2.mdx mice display significantly reduced average track length covered in 30 min, % of time spent active and number of rearings during the 30 min in the open field compared with the B10.mdx strain and their respective parental strain controls.

3.2. Assess the skeletal muscle regenerative capacity in a survey of 16 inbred background strains and create two congenic mdx strains on the backgrounds with the lowest regenerative capacity.

Based on the significant increase in severity and the acceleration of disease symptoms we have discovered in the D2.B10-*Dmd*^{mdx} congenic strain described above (**Figures 2 and 3**) and in **Figure 4** (below), future work will more rapidly develop additional *mdx* mouse models for phenotypic analysis. We plan to utilize a CRISPER/Cas9 approach to target exon 23 of the mouse *Dmd* gene to create a series of DMD mouse models directly on eight additional genetically diverse mouse strains. The eight strains are A/J, C57BL/6J, 129S1/SvImJ, NOD/LtJ, NZO/HILtJ, CAST/EiJ, PWK/PhJ, and WSB/EiJ. These strains will allow us to capture nearly 90% of the known variation present in laboratory mice as potential genetic modifiers of disease. In addition, these strains have an additional advantage as they have been used to develop sophisticated genetic reference populations from an 8-way cross of these founder strains - the Collaborative Cross (CC) and Diversity Outcross (DO) populations. The use of CC and DO populations will facilitate genetic mapping and phenotypic confirmation of any potential modifier loci that might control disease pathology.

3.3. Genetically map quantitative trait locus modifiers of mdx phenotypic severity derived from the DBA/2J background in an N2 backcross population of C57BL/6J x D2.B10-mdx mice.

The mapping cross was modified to utilize an F2 intercross that has greatly increased the genetic resolution of the map to speed the discovery of genetic recombinants. The significant enhancement of muscular dystrophy symptoms observed on the DBA/2J background (mild vs. severe) will allow us to better discriminate phenotypic variation such that additive effects that might be apparent in an intercross to aid in identifying additional modifier loci.

Aim 4. Test promising therapeutic compounds in the preclinical DBA/2J-*mdx* congenic model.
K. Nagaraju, CNMC.

Overview

As outlined in Aim 4 of the grant proposal, we have established a D2.MDX colony and carried out an extensive characterization of this mouse using a battery of behavioral, functional, and histological measures (See Manuscript submitted for publication in Appendix 1). We have compared the D2.MDX mice to their B10.MDX counterparts, as well as both relevant control strains for up to one year. This extensive comparison allows us to state that the D2.MDX mice do indeed possess a more severe muscular dystrophy than the commonly used B10.MDX strain. Our work has also identified multiple measurable outcomes in D2.MDX that may be assessed at earlier time points. Consequently, the D2.MDX model of Duchenne muscular dystrophy (DMD) could potentially reduce the time required to carry out an animal study by half.

Aim 4.1 Results: For comparisons, D2.MDX mice were compared to B10.MDX mice and respective DBA2 and C57Bl10 control strains at three different time points (1.5 months, 7 months, and 12

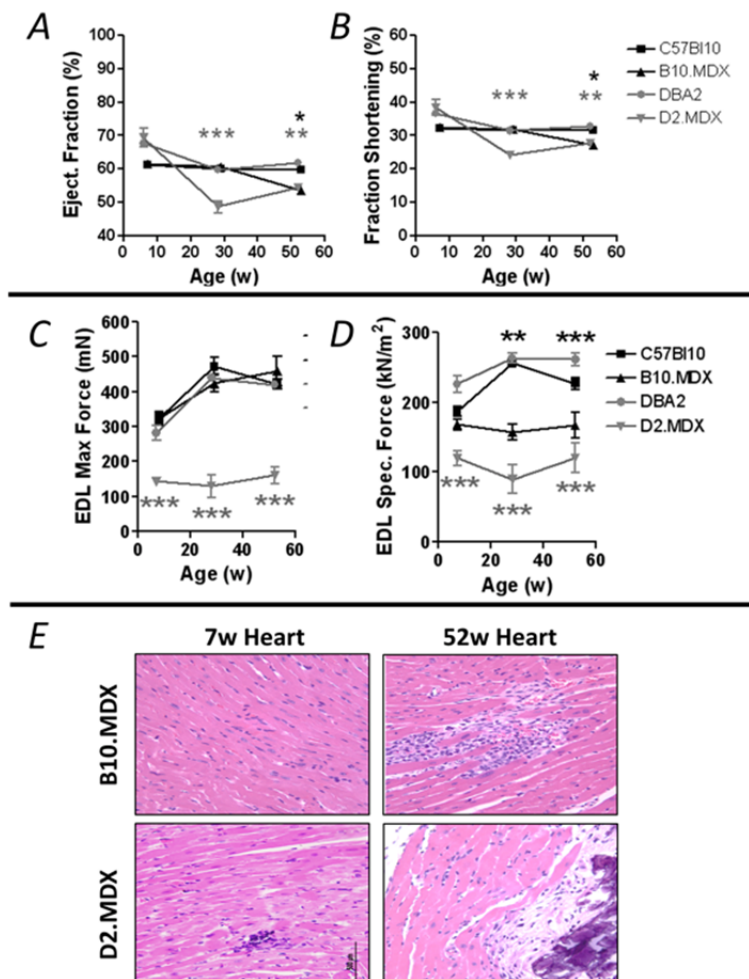


Figure 4. A total of four mouse strains (C57Bl10, B10.MDX, DBA2, D2.MDX) were compared extensively at three time points (7, 28, and 52 weeks). Echocardiography revealed that the D2.MDX strain had significant deficits in cardiac performance at 28 and 52 weeks of age both in terms of the ejection fraction (A) and the shortening fraction (B). Skeletal muscle strength was also significantly reduced in the D2.MDX strain at all ages (C) although the specific force generated was not seen to be weaker until the animals were at least 28 weeks old (D). Representative histological findings from the heart of D2.MDX and B10.MDX mice at both 7 weeks and 52 weeks old are shown in panel E. The early appearance of damage in the D2.MDX heart is consistent with the loss in cardiac performance. In summary, the D2.MDX mice show an accelerated and more severe pathology compared to the commonly used B10.MDX strain.

months). The full results have been drafted into a manuscript and is currently under revision for Human Molecular Genetics. The most novel findings were made during our assessment of cardiac performance, our assessment of muscle function, and our examinations of muscle histology.

Cardiac performance: The results from our echocardiography indicated that the D2.MDX mice suffer from a drop in cardiac performance as early as 7 months of age. This is an accelerated pathology compared to the common B10.MDX model that requires up to 12 months before any cardiomyopathy become apparent. Furthermore, the D2.MDX cardiomyopathy is already more severe at 7 months compared to B10.MDX mice. These striking results are seen in part in **Figure 4A and 4B**. This rapid heart damage makes the D2.MDX mouse a superior model for testing drugs that may improve heart performance.

Skeletal muscle function: Our quantitative assessment of muscle function is a very sensitive and powerful technique. Our results show that there is a dramatic loss of muscle strength in the D2.MDX mice compared to any other mouse strain at any age. A portion of these results are shown in **Figure 4C and 4D**. This weakness is measurable both in terms of the total force generated, and force generated per volume of muscle mass. This weakness also appears in the D2.MDX much earlier than in the B10.MDX mice. Again, the severity and accelerated course of disease symptoms in the D2.MDX mice makes this new model a superior choice for animal drug trials.

Muscle histology: The most striking feature visible in the muscle histology of D2.MDX mice is the appearance of calcified lesions within the skeletal muscle as early as 1.5 months of age. Similar lesions do not appear in B10.MDX animals until a year or later. A few representative images from the 1.5 month old animals are shown in **Figure 4E**. The majority of the data does not suggest that the inflammatory response is significantly different between the two strains, thereby suggesting that the appearance of these calcium deposits is due to innate differences in muscle fiber death and clearance within the muscle tissue. It must also be noted that at 1.5 months of age the D2.MDX23 mice show cardiac fiber degeneration and calcification centered over the right ventricle epicardium. This unusual pathology was not seen in B10.MDX animals even up to 12 months in age. Overall, these results reinforce the conclusion that compared to B10.MDX mice the D2.MDX cardiomyopathy is accelerated and more severe.

C. KEY RESEARCH ACCOMPLISHMENTS

- We have established an MD Repository at The Jackson Laboratory that has actively solicited critical models of human muscular dystrophy.
- We have imported and re-derived fifteen lines of mice (Aim 1) into the MD Repository to add to our over 20 models of muscular dystrophy that were available at the start of this proposal.
- Genetic and phenotypic information regarding all new lines of mice have been posted to the JAX website and will soon be consolidated into a dedicated page for muscular dystrophy models.
- We have generated full-length and internally truncated human dystrophin constructs for inclusion in targeted transgenic experiments that will test the potential efficacy of antisense oligonucleotide therapies to induce deletions of exons 44-45, 49-51, 48-53.
- We have created a D2.B10-*Dmd*^{mdx} congenic strain of mice using a speed congenic protocol that shows significant muscle pathology.
- We have shown that D2.B10-*Dmd*^{mdx} congenic mice display more severe dystrophy symptoms than the original B10- *Dmd*^{mdx} strain and also display unique cardiomyopathy features that are likely to be relevant to the human disease.

D. REPORTABLE OUTCOMES

Abstracts and presentations

- 2011 Muscle Study Group meeting, Rochester, NY. **C Lutz**, JAX
- 2011 Parent Project Muscular Dystrophy, West Coast CONNECT meeting, San Diego, CA. **K. Nagaraju**, CNMC
- 2011 Myositis/Myopathy study group at the ACR annual meeting, Washington DC. **K. Nagaraju**, CNMC
- 2011 LGMD2A workshop sponsored by the Coalition to cure calpain3, Santa Monica, CA. **K. Nagaraju**, CNMC
- 2011 Fourth annual programs in Clinical and Translational Research: Muscular Dystrophy and Rehabilitation Medicine Programs in Clinical and Translational Research: Muscular Dystrophy and Rehabilitation Medicine, Washington DC. **K. Nagaraju**, CNMC
- 2011 Fifth annual dysferlin conference, Chicago, IL. **K. Nagaraju**, CNMC
- 2011 Oral presentation at the Jain foundation meeting. Chicago, IL. "Role of Toll-Like Receptors (TLRs) in the Pathogenesis of Dysferlin Deficiency." **K. Nagaraju**, CNMC
- 2012 2012 international conference, organized by Duchenne parent project, Italy in Feb 17th-Feb19th Rome, Italy. **K. Nagaraju**, CNMC
- 2012 32nd European Workshop for Rheumatology Research (EWRR) on February 23rd-25th, 2012, in Stockholm. **K. Nagaraju**, CNMC.
- 2012 Myomatrix 2012 meeting at University of Nevada, Reno, April 22nd-24th 2012. **G Cox**, JAX and **K. Nagaraju**, CNMC.
- 2012 Dr **Lutz** attended and presented at the Phacillitate Rare Disease Leaders Forum in San Francisco
- 2013 Dr. **Lutz** and Dr. **Nagaraju** attended and participated in the workshop Developing Rigor in Congenital Muscle Disease Preclinical Testing in Washington DC.
- 2013 Dr. **Lutz** and Dr. **Nagaraju** attended and presented talks at the Muscular Dystrophy Association Meeting in Washington DC.
- 2013 Quinn, J., Huynh T., Uaesoontrachoon K., Tatem K., Phadke A., Vandermeulen J., Yu Q., **Nagaraju**, K. (2013) Effects of Dantrolene Therapy on Disease Phenotype in Dystrophin Deficient mdx Mice. MDA Scientific Conference, Washington DC
- 2013 Dr **Lutz** attended and presented at the Neuroscience Meeting in San Diego, CA.
- 2013 Dr. **Lutz** and Dr. **Nagaraju** attended and participated in the workshop Developing Rigor in Congenital Muscle Disease Preclinical Testing in Washington DC.
- 2013 Dr. **Lutz** and Dr. **Nagaraju** attended and presented talks at the Muscular Dystrophy Association Meeting in Washington DC.
- 2014 Dr. **Lutz** and Dr. **Nagaraju** attended and presented talks at the Muscular Dystrophy Association Meeting in Washington DC.
- 2015 Dr. **Lutz** and Dr. **Nagaraju** presented a poster at MDA Scientific conference in Washington DC, March 11-14.

Manuscripts

- Jahnke V, VanderMeulen J, Johnston H, Partridge T, Hoffman EP and **Nagaraju K**. Metabolic remodeling agents (AMPK and peroxisome proliferator activated receptor δ agonists) show beneficial effects in the dystrophin deficient mdx mouse model. **Skelet Muscle**. 2012 Aug 21;2(1):16. doi: 10.1186/2044-5040-2-16.
- Coley WD, Bogdanik L, Yu Q, van der Meulen JH, Rayavarapu S, Quinn JL, Saunders A, Dolan C, Vila MC, Andrews W, Lammert C, Austin A, Partridge T, **Cox GA**, **Lutz C**, **Nagaraju K**. Effect of genetic background on the dystrophic phenotype in *mdx* mice. Hum Mol Gen (In Revision).

E. CONCLUSION:

The development of an MD Repository has significantly increased the availability of high-demand strains of mice for research and will allow standardization of genetic background and genetic quality control to facilitate academic and pharmaceutical adoption of these strains for translational studies. We have established outreach into the muscular dystrophy research and clinical community (congenital muscle disease consortium) to determine the models most anticipated for preclinical research and we are actively soliciting those models for inclusion in the repository. In Aim 2, our transgenic experiments to express in-frame deleted forms of dystrophin will model the best-case-scenario outcome for AO-mediated therapy in which one assumes that a particular compound is capable of 100% effective exon-skipping to restore the reading frame. By eliminating all of the caveats regarding the efficiency of delivery and pharmacodynamics of the particular therapeutic, we can provide a model that will allow functional analysis of the extent of phenotypic rescue for the three most common in-frame deletions for which clinical information from human Becker muscular dystrophy patients (deletion of exons 44-45, 49-51, 48-53) is lacking. In Aims 3 and 4, we have created a novel D2.B10-mdx congenic strain of mice that appears to be a better preclinical model of disease with an increased severity of myopathic symptoms for better outcome measures in preclinical drug studies. These congenic mice will also provide the starting point for a genetic modifier screen to identify genes and pathways that affect disease severity.

Curriculum Vitae

Gregory A. Cox

Office Address:

The Jackson Laboratory
600 Main Street
Bar Harbor, ME 04609
Fax: (207) 288-6077
Email: greg.cox@jax.org

Personal Data:

Education:

1984–1989	B.S., Humboldt State University, Arcata, CA Summa Cum Laude with Distinction Biology–Cellular/Molecular
1989–1994	Ph.D., University of Michigan, Conferred Dec. 18, 1994 Department of Human Genetics Jeffrey S. Chamberlain, Ph.D., Thesis Advisor
1994–1999	Postdoctoral Research, The Jackson Laboratory, Bar Harbor, ME Wayne N. Frankel, Ph.D., Advisor
1999–2006	Associate Staff Scientist/Assistant Professor, The Jackson Laboratory
2006–present	Staff Scientist/Associate Professor, The Jackson Laboratory

Awards and Honors:

1988	Fred Telonicher Memorial Award, Humboldt State University.
1989–1990	NIH Predoctoral Genetics Training Grant, University of Michigan.
1991–1993	National Science Foundation (NSF) Predoctoral Fellowship, University of Michigan.
1994	Distinguished Dissertation Award, University of Michigan.
1994–1995	NIH Developmental Genetics Postdoctoral Training Grant, The Jackson Laboratory.

Research Fellowships and Grants:

1995–1997	National Research Service Award (NRSA) NIH Postdoctoral Fellowship, The Jackson Laboratory.
1997–1998	National Research Service Award (NRSA) NIH Postdoctoral Fellowship, Competitive Renewal, The Jackson Laboratory.
1997–1998	Amyotrophic Lateral Sclerosis (ALS) Association Research Grant, “Identifying the mutation and a major genetic modifier of neuromuscular degeneration” (P.I.)
1998–2001	Amyotrophic Lateral Sclerosis (ALS) Association Research Grant, “Genetic mechanisms of neuromuscular degeneration” (P.I.).
1998–2002	NIH/NINDS “Genetic control of neuromuscular degeneration” (P.I.).

2000-2003	Amyotrophic Lateral Sclerosis Association , “Identification of Genetic Modifiers for Amyotrophic Lateral” (P.I.)
2001-2002	Johns Hopkins Center for ALS Research , "Mapping the Hereditary 2000-2005 NIH/NINDS, "Production and Screening of Mouse Neurological Mutations" (P.I.)
2001-2005	NIH/NIA, "Genetic Locus Extending Life and Reducing Insulin"(Co-P.I.)
2001-2005	NIH/NIA, “Regulation of Hyper Hemopoietic Stem Cell Function” (Co-P.I.)
2002-2007	NIH/NINDS “Molecular Genetics of Muscular-Neurosensory Models” (Co-P.I.).
2003-2008	NIH/NIAMS “Genetic Mechanisms of Muscular Dystrophy in Mice” (P.I.)
2004-2007	Amyotrophic Lateral Sclerosis Association, “ALS Model Development at The Jackson Laboratory” (Co-P.I.).
2004-2012	NIH/NIAMS “Cpdm: Cloning A Gene That Regulates Eosinophil Function” (Co-P.I.)
2007-2012	NIH/NINDS “Genetics of the Neuromuscular Junction: Mechanisms and Disease Models” (Co-P.I.)
2007-2008	MIHGH Seed Grant “Generating Mouse Models of Familial Paranganglioma” (P.I.)
2007-2011	NIH/NINDS “Genetic Control of RNA Metabolism: Analysis of the SMARD 1 Helicase” (Co-P.I.).
2012-2013	ALS Association “Nuclear/cytoplasmic trafficking defects in motor neuron disease models.” (P.I.)
2013-2015	NIH/NINDS R21 "Metabolite Profiling of a Novel Mitochondrial Kinase in Neuromuscular Disease" (Multiple P.I.)
2013-2015	NIH/NINDS R21 " Imaging Circuit Change in the Motor Cortex of Mouse Model of ALS" (P.I.)
2007-2017	NIH/NIAMS “Genetic control of phospholipid biosynthesis and muscular dystrophy” (P.I.)

Publications:

1. Chamberlain JS, Farwell NJ, Ranier JE, **Cox GA**, Caskey CT. 1991. PCR analysis of dystrophin gene mutation and expression. *J. Cell Biochem.* 46: 255–259.
2. **Cox GA**, Phelps SF, Chapman VM, Chamberlain JS. 1993. New *mdx* mutation disrupts expression of muscle and nonmuscle isoforms of dystrophin. *Nature Genetics* 4: 87–93.
3. **Cox GA**, Cole NM, Matsumura K, Phelps SF, Hauschka SD, Campbell KP, Faulkner JA, Chamberlain JS. 1993. Overexpression of dystrophin in transgenic *mdx* mice eliminates dystrophic symptoms without toxicity. *Nature* 364: 725–729.
4. Denetclaw WF, Jr., Hopf FW, **Cox GA**, Chamberlain JS, Steinhardt RA. 1994. Myotubes from transgenic *mdx* mice expressing full-length dystrophin show normal calcium regulation. *Mol. Biol. Cell* 5: 1159-1167.
5. **Cox GA**, Sunada Y, Campbell KP, Chamberlain JS. 1994. Dp71 can restore the dystrophin-associated glycoprotein complex in muscle but fails to prevent dystrophy. *Nature Genetics* 8: 333–339.

6. Rafael JA, **Cox GA**, Corrado K, Jung D, Campbell KP, Chamberlain JS. 1996. Forced expression of dystrophin deletion constructs reveals structure-function correlations. *J. Cell Biol.* 134: 93-102.
7. **Cox GA**, Lutz CM, Yang C-L, Biemesderfer D, Bronson RT, Fu A, Aronson PS, Noebels JL, Frankel WN. 1997. Sodium/hydrogen exchanger gene defect in slow-wave epilepsy mutant mice. *Cell* 91: 139-148.
8. **Cox GA**, Mahaffey CL, Frankel WN. 1998. Identification of the mouse neuromuscular degeneration gene and mapping of a second site suppressor allele. *Neuron* 21: 1327-1337
9. Lumeng CN, Phelps SF, Rafael JA, **Cox GA**, Hutchinson TL, Begy CR, Adkins E, Wiltshire R, Chamberlain JS. 1999. Characterization of dystrophin and utrophin diversity in the mouse. *Hum. Mol. Genet.* 8:593-599.
10. **Cox GA**, Mahaffey CL, Nystuen A, Letts VA, Frankel WN. 2000. The mouse fidgetin gene defines a new role for AAA family proteins in mammalian development. *Nature Genetics* 26: 198-202.
11. Sundberg JP, Boggess D, Shultz LD, Fijneman RJ, Demant P, HogenEsch H, **Cox GA**. 2000. The chronic proliferative dermatitis mouse mutation (*cpdm*): mapping of the mutant gene locus. *J. Exp. Anim. Sci.* 41: 101-108.
12. Garvey SM, Rajan, C, Lerner AP, Frankel WN, **Cox GA**. 2002. The Muscular Dystrophy with myositis (*mdm*) mouse mutation disrupts a skeletal muscle-specific domain of titin. *Genomics* 79: 146-149.
13. Sundberg JP, Boggess D, Silva KA, McElwee KJ, King LE, Li R, Churchill G, Cox GA. 2003. Major locus on mouse chromosome 17 and minor locus on chromosome 9 are linked with alopecia areata in C3H/HeJ mice. *J. Invest. Dermatol.* 120: 771-775.
14. Serreze DV, Pierce MA, Post CM, Chapman HD, Savage H, Bronson RT, Rothman PB, **Cox GA**. 2003. Paralytic autoimmune myositis develops in addition to type 1 diabetes in NOD mice made Th1 cytokine deficient by expression of an IFN γ receptor β chain transgene. *J. Immunology* 170: 2742-2749.
15. Maddatu TP, Garvey SM, Shroeder DG, Hampton TG, **Cox GA**. 2004. Transgenic rescue of neurogenic atrophy in the *nmd* mouse reveals a role for *Ighmbp2* in dilated cardiomyopathy. *Hum. Mol. Genet.* 13: 1105-1115.
16. Sundberg JP, Silva KA, Li R, **Cox GA**, King LE. 2004. Adult onset alopecia areata is a complex polygenic trait in the C3H/HeJ mouse model. *J. Invest. Dermatol.* 123: 294-297.
17. Ho M, Post CM, Donahue LR, Lidov HGW, Bronson RT, Goolsby H, Watkins SC, **Cox GA**, Brown RH Jr. 2004. Disruption of muscle membrane and phenotype divergence in two mouse models of dysferlin-deficiency. *Hum. Mol. Genet.* 13: 1999-2010.
18. Wooley, CM, Sher, RB, Frankel, WN, **Cox, GA**, and Seaburn, KL. 2005. SOD1 mice have subtle gait defects prior to the appearance of overt symptoms. *Muscle and Nerve* 32: 43-50.
19. Lee Y, Kameya S, **Cox GA**, Hsu J, Hicks W, Maddatu TP, Smith RS, Naggert JK, Peachey NS, and

- Nishina PM. 2005. Ocular abnormalities in *Large^{myd}* and *Large^{vis}* mice, spontaneous models for muscle, eye, brain diseases. *Mol. Cell Neurosci.* 30: 160-172.
20. Huebsch KA, Kudryashova E, Wooley CM, Sher RB, Seburn KL, Spencer MJ, **Cox GA**. 2005. mdm Muscular Dystrophy: Interactions with Calpain 3 and a Novel Functional Role for Titin's N2A Domain. *Hum. Mol. Genet.* 14: 2801-2811.
 21. Maddatu, TP, Garvey, SM, Schroeder, DG, Zhang, W, Kim, S-Y, Nicholson, AI, Davis, CJ, **Cox, GA**. 2005. Dilated cardiomyopathy (DCM) in the *nmd* mouse: Transgenic rescue and QTLs that improve cardiac function and survival. *Hum. Mol. Genet.* 14: 3179-3189.
 22. Tarchini B, Hanh T, Huynh N, **Cox GA** and Duboule D. 2005. *HoxD* cluster scanning deletions identify multiple defects leading to paralysis in the mouse mutant *Ironside*. *Genes Dev.* 19: 2862-2876.
 23. Hadano, S, Benn, SC, Kakuta S, Otomo, A, Sudo, K, Kunita, R, Suzuki-Utsunomiya, K, Mizumura, H, Shefner, JM, **Cox, GA**, Iwakura, Y, Brown, RH Jr, Ikeda, J-E. 2006. Mice Deficient in the Rab5 Guanine Nucleotide Exchange Factor ALS2/alsin Exhibit Age-Dependent Neurological Deficits and Altered Endosome Trafficking. *Hum. Mol. Genet.* 15: 233-250.
 24. Mikaelian, I, Hovick, M, Silva, KA, Burzenski, LM, Shultz, LD, Ackert-Bicknell, CL, **Cox, GA**, Sundberg, JP. 2006. Expression of terminal differentiation proteins defines stages of mouse mammary gland development. *Vet. Pathol.* 43: 36-49.
 25. Sher, RB, Aoyoma, C, Huebsch KA, Ji, S, Kerner, K, Yang, Y, Frankel, WN, Hoppel, CL, Wood, PA, Vance, DE, **Cox, GA**. 2006. A rostrocaudal muscular dystrophy caused by a defect in choline kinase beta, the first enzyme in phosphatidylcholine biosynthesis. *J. Biol. Chem.* 281: 4938-4948.
 26. Runkel, F, Büsow, H, Seburn KL, **Cox, GA**, McVeigh Ward, D, Kaplan, J, Franz, T. 2006. *Grey*, a novel mutation in the murine *Lyst* gene causes the *beige* phenotype by skipping of exon 25. *Mamm. Genome* 17: 203-210.
 27. Seburn, KL, Nangle, LA, **Cox, GA**, Schimmel, P, Burgess, RW. 2006. A mouse model of Charcot Marie Tooth 2D indicates sensory and motor neuropathy and a novel pathogenic function for the mutant protein. *Neuron* 51: 715-726.
 28. Yang, Y, Mahaffey, CL, Maddatu, TP, **Cox, GA**, Graber, JH, Frankel, WN. 2007. Deficiency in a brain specific RNA binding protein leads to seizures in a novel mouse model of epilepsy. *PLoS Genetics* 3: 1275-1283.
 29. Seymour RE, Hasham MG, **Cox GA**, Shultz LD, Hogenesch H, Roopenian DC, Sundberg JP. 2007. Spontaneous mutations in the mouse Sharpin gene result in multiorgan inflammation, immune system dysregulation and dermatitis. *Genes Immun.* 8: 416-421.
 30. Cohen TJ, Waddell DS, Barrientos T, Lu Z, Feng G, **Cox GA**, Bodine SC, Yao TP. 2007. The histone deacetylase HDAC4 connects neural activity to muscle transcriptional reprogramming. *J. Biol. Chem.* 282: 33752-33759.

31. Maltecca F, Aghaie A, Schroeder DG, Cassina L, Taylor BA, Phillips SJ, Malaguti M, Previtali S, Guénet JL, Quattrini A, **Cox GA**, Casari G. 2008. The mitochondrial protease AFG3L2 is essential for axonal development. *J. Neurosci.* 28: 2827-2836.
32. Lopez MA, Pardo P, **Cox GA**, Boriek AM. 2008. Early Mechanical Dysfunction of the Respiratory Pump in the Muscular Dystrophy with Myositis (*Ttn^{mdm}*) Model. *Am. J. Physiol. Cell Physiol.* 295: C1092-1102.
33. Walters BJ, Campbell SL, Chen PC, Taylor AP, Schroeder DG, Dobrunz LE, Artavanis-Tsakonas K, Ploegh HL, Wilson JA, **Cox GA**, Wilson SM. 2008. Differential effects of Usp14 and Uch-L1 on the ubiquitin proteasome system and synaptic activity. *Mol. Cell. Neurosci.* 39:539-548.
34. Cohen TJ, Barrientos T, Garvey SM, Hartman ZC, **Cox GA**, Bedlack RS, Yao TP. 2009. The deacetylase HDAC4 controls myocyte enhancing factor-2-dependent structural gene expression in response to neural activity. *FASEB J.* 23:99-106.
35. Wooley CM, Xing S, Burgess RW, **Cox GA**, Seburn KL. 2009. Age, experience and genetic background influence treadmill walking in mice. *Physiol Behav.* 96: 350-361.
36. Wu G, Sher RB, **Cox GA**, Vance DE. 2009. Understanding the muscular dystrophy caused by deletion of choline kinase beta in mice. *Biochim Biophys Acta.* 1791: 347-356.
37. Martinelli P, La Mattina V, Bernacchia A, Magnoni R, Cerri F, **Cox G**, Quattrini A, Casari G, Rugarli EI. 2009. Genetic interaction between the m-AAA protease isoenzymes reveals novel roles in cerebellar degeneration. *Hum. Mol. Genet.* 18: 2001-2013.
38. de Planell-Saguer M, Schroeder DG, Rodicio MC, **Cox GA**, Mourelatos Z. 2009. Biochemical and genetic evidence for a role of IGHMBP2 in the translational machinery. *Hum. Mol. Genet.* 18: 2115-2126.
39. Maltecca F, Magnoni R, Cerri F, **Cox GA**, Quattrini A, Casari G. 2009. Haploinsufficiency of *AFG3L2*, the gene responsible for spinocerebellarataxia type 28 (SCA28), causes mitochondria-mediated Purkinje cell dark degeneration. *J. Neurosci.* 29: 9244-9254.
40. Chase TH, **Cox GA**, Burzenski L, Foreman O, Shultz LD. 2009. Dysferlin deficiency and the development of cardiomyopathy in a mouse model of limb-girdle muscular dystrophy 2B. *Am J Pathol.* 175: 2299-2308.
41. Lee BJ, **Cox GA**, Maddatu TP, Judex S, Rubin CT. 2009. Devastation of bone tissue in the appendicular skeleton parallels the progression of neuromuscular disease. *J Musculoskelet Neuronal Interact.* 9: 215-224.
42. Wu G, Sher RB, **Cox GA**, Vance DE. 2010. Differential Expression of Choline Kinase Isoforms in Skeletal Muscle Explains the Phenotypic Variability in the Rostrocaudal Muscular Dystrophy Mouse. *Biochim. Biophys. Acta.* 1801: 446-454.
43. Burgess RW, **Cox GA**, Seburn KL. 2010. Neuromuscular disease models and analysis. *Methods Mol. Biol.* 602: 347-393.
44. Mohamed JS, Lopez MA, **Cox GA**, Boriek AM. 2010. Anisotropic regulation of Ankrd2 gene expression in skeletal muscle by mechanical stretch. *FASEB J.* 24: 3330-3340.

45. Heiman-Patterson TD, Sher RB, Blankenhorn EA, Alexander G, Deitch JS, Kunst CB, Figlewicz D, Maragakis N, **Cox GA**. 2011. Effect of Genetic Background on Phenotype Variability in Transgenic Mouse Models of Amyotrophic Lateral Sclerosis: A window of opportunity in the search for genetic modifiers. *Amyotroph Lateral Scler.* 12:79-86.
46. Mitsuhashi S, Ohkuma A, Talim B, Karahashi M, Koumura T, Aoyama C, Kurihara M, Quinlivan R, Sewry C, Mitsuhashi H, Goto K, Koksai B, Kale G, Ikeda K, Taguchi R, Noguchi S, Hayashi YK, Nonaka I, Sher RB, Sugimoto H, Nakagawa Y, **Cox GA**, Topaloglu H, Nishino I. 2011. A novel congenital muscular dystrophy with mitochondrial structural abnormalities caused by defective *de novo* phosphatidylcholine biosynthesis. *Am. J. Hum Gen.* 88:845-851.
47. Sher RB, **Cox GA**, Mills KD, Sundberg JP. Rhabdomyosarcomas in Aging A/J Mice. 2011. *PLoS One.* 6(8):e23498.
48. Mitsuhashi S, Hatakeyama H, Karahashi M, Koumura T, Nonaka I, Hayashi YK, Noguchi S, Sher RB, Nakagawa Y, Manfredi G, Goto YI, **Cox GA**, Nishino I. 2011. Muscle choline kinase beta defect causes mitochondrial dysfunction and increased mitophagy. *Hum Mol. Genet.* 20:3841-3851.
49. Su YQ, Sugiura K, Sun F, Pendola JK, **Cox GA**, Handel MA, Schimenti JC, Eppig JJ. 2012. MARF1 regulates essential oogenic processes in mice. *Science.* 335(6075):1496-1499.
50. Strokin M, Seburn KL, **Cox GA**, Martens KA, Reiser G. 2012. Severe disturbance in the Ca²⁺ signaling in astrocytes from mouse models of human infantile neuroaxonal dystrophy (INAD) with mutated Pla2g6. *Hum Mol Genet.* 21:2807-2814.
51. Choi MC, Cohen TJ, Barrientos T, Wang B, Li M, Simmons BJ, Yang JS, **Cox GA**, Zhao Y, Yao TP. 2012. A Direct HDAC4-MAP Kinase Crosstalk Activates Muscle Atrophy Program. *Mol Cell.* 13:122-132.
52. Hosur V, Riefler J, Lyons B, Gott B, Carney L, Kavirayani A, **Cox, GA**, Shultz LD. 2012. Dystrophin and Dysferlin Double Mutant Mice: A Novel Model for Rhabdomyosarcoma. *Cancer Genetics.* 205:232-241.
53. Hoffman EP, Gordish-Dressman H, McLane VD, Devaney JM, Thompson PD, Visich P, Gordon PM, Pescatello LS, Zoeller RF, Moyna NM, Angelopoulos TJ, Pegoraro E, **Cox GA**, Clarkson PM. 2012. Alterations in Osteopontin Modify Muscle Size in Females in Both Humans and Mice. *Med Sci Sports Exerc.* 45:1060-8.
54. Hosur V, Cox ML, Burzenski LM, Riding RL, Alley L, Lyons BL, Kavirayani A, Martin KA, **Cox GA**, Johnson KR, Shultz LD. 2013. Retrotransposon insertion in the T-cell acute lymphocytic leukemia 1 (Tal1) gene is associated with severe renal disease and patchy alopecia in Hairpatches (Hpt) mice. *PLoS One.* 8:e53426.

55. Mohamed JS, Lopez MA, **Cox GA**, Boriek AM. 2013. Ankyrin Repeat Domain Protein 2 and Inhibitor of DNA Binding 3 Cooperatively Inhibit Myoblast Differentiation by Physical Interaction. *J. Biol. Chem.* 288:24560-8.
56. Li Z, Wu G, Sher RB, Khavandgar Z, Hermansson M, **Cox GA**, Doschak MR, Murshed M, Beier F, Vance DE. 2014. Choline kinase beta is required for normal endochondral bone formation. *Biochim Biophys Acta.* S0304-4165(14)00112-3.
57. Sher RB, Heiman-Patterson TD, Blankenhorn EA, Jiang J, Alexander G, Deitch JS, **Cox GA**. 2014. A major QTL on mouse chromosome 17 resulting in lifespan variability in SOD1-G93A transgenic mouse models of amyotrophic lateral sclerosis. *Amyotroph Lateral Scler.* 15(7-8):588-600.
58. Heiman-Patterson TD, Blankenhorn EP, Sher RB, Jiang J, Welsh P, Dixon MC, Jeffrey JI, Wong P, **Cox GA**, Alexander GM. Genetic Background Effects on Disease Onset and Lifespan of the Mutant Dynactin p150Glued Mouse Model of Motor Neuron Disease *Plos One* 10(3):e0117848.
59. Fairfield H, Srivastava A, Ananda G, Liu R, Kircher M, Lakshminarayana A, Harris BS, Karst SY, Dionne LA, Kane CC, Curtain M, Berry ML, Ward-Bailey PF, Greenstein I, Byers C, Czechanski A, Sharp J, Palmer K, Gudis P, Martin W, Tadenev A, Bogdanik L, Pratt CH, Chang B, Schroeder DG, **Cox GA**, Cliften P, Milbrandt J, Murray S, Burgess R, Bergstrom DE, Donahue LR, Hamamy H, Masri A, Santoni FA, Makrythanasis P, Antonarakis SE, Shendure J, Reinholdt LG. 2015. Exome sequencing reveals pathogenic mutations in 91 strains of mice with Mendelian disorders. *Genome Res.* 25(7):948-57.

Books, Book Chapters and Reviews

60. Chamberlain JS, Phelps SF, **Cox GA**, Maichele AJ, Greenwood AD. 1993. PCR analysis of muscular dystrophy in *mdx* mice. In: *Molecular and Cell Biology of Muscular Dystrophy*, Partridge T (ed), Chapman & Hall. 167-189.
61. Chamberlain JS, Corrado K, Rafael JA, **Cox GA**, Hauser M, Lumeng C. 1997. Interactions between dystrophin and the sarcolemma membrane. In: *Cytoskeletal Regulation of Membrane Function* (ed. Froehner SC and Bennett V, The Rockefeller University Press, New York): 19-29.
62. Ackerman, SL and **Cox, GA**. 2008. From ER to Eph receptors: new roles for VAP fragments. *Cell* 133: 949-951.

Teaching:

TJL Courses

Short Course on Medical and Experimental Mammalian Genetics, 2012-Present.
 Experimental Genetics of the Laboratory Mouse in Cancer Research. 1998-2012.
 TJL Kids' Science Night. Summer, 1998-2001.
 Genome Sequence Analysis: Theory and Practice. June, 2002.
 Short Course on Pathobiology of the Modern Laboratory Mouse. 2002-2003.

U Maine Courses

BMB550 Special Topics in Molecular Biology: Animal Models for Biomedical Research. "Mouse Genetics" University of Maine, Orono. Department of Biochemistry, Microbiology and Molecular Biology, November, 2002. 1.5 classroom hours.

BMB550 Special Topics in Molecular Biology: Animal Models for Biomedical Research. “Mouse Genetics” University of Maine, Orono. Department of Biochemistry, Microbiology and Molecular Biology, September, 2004. 1.5 classroom hours.

BMB550 Special Topics in Molecular Biology: Functional Genomics. “Mouse models of genetic disease” University of Maine, Orono. Department of Biochemistry, Microbiology and Molecular Biology, 2004-Present. 3 classroom hours/year.

BMS525 Molecular Genetics, University of Maine, Orono. Graduate School of Biomedical Science and Engineering, 2105. 1.5 classroom hours/year.

Tufts Courses

GENE 205B: Mammalian Genetics, 2012-Present.

TJL Summer and Academic Year Students

Catherine Del Vecchio, John Bapst High School, Bangor, ME. TJL Summer Student Program (2000).
 Rachel Lee, Maine School of Science and Math, Limestone, ME. TJL Summer Student Program (2000).
 Amy Russell, MDI High School, Bar Harbor, ME. High School Internship Program. (2000-2002).
 Jesse Mynahan, Poland Regional High School, Poland, ME. TJL Summer Student Program (2001).
 Jilian Sacks, Dartmouth College, Hanover, NH. College Semester Intern (2001).
 Rebecca C. Edgerly, Leominster High School, Leominster, MA. TJL Summer Student Program (2002).
 Eva Murdock, John Bapst High School, Bangor, ME. High School Intern (2002).
 Alexandra Kieffer, Marquette High School, Bellevue, IA. TJL Summer Student Program (2003).
 Michael Birnbaum, Central High School, Philadelphia, PA. TJL Summer Student Program (2003).
 Ashley Taylor, Oberlin College, Oberlin, OH. TJL Summer Student Program (2004).
 Innocent Ndzana, University of Maine, Machias, ME. TJL Summer Student Program (2005).
 Laura Supkoff, Brown University, Providence, RI. TJL Summer Student Program (2005).
 Jon Gridley, MDI High School, Bar Harbor, ME. High School Internship Program. (2005).
 Alexandra Landry, NC Science and Mathematics, Durham, NC. TJL Summer Student Program (2006).
 Seanna Pieper-Jordan, Kamehameha High School, Honolulu, HI. TJL Summer Student Program (2007).
 Nina Peterson, MDI High School, Bar Harbor, ME. High School Internship Program. (2008).
 Alex Royce, MDI High School, Bar Harbor, ME. High School Internship Program. (2007-2009).
 Destiny Kanu, MDI High School, Bar Harbor, ME. High School Internship Program. (2009-2010).
 Kate Macina, NYU, New York, NY. JAX Summer Student Program (2010).
 Rebecca Edgecomb, MDI High School, Bar Harbor, ME. High School Internship Program. (2010-2011).
 Anastasia Singalevich, Hebrew University, Jerusalem, Israel. JAX Summer Student Program (2011).
 Chelsea Culbert, NYU, New York, NY. JAX Summer Student Program (2011).
 Elisabeth Adkins, Tufts/JAX Graduate Student Rotation (2012).
 Conner Foster, Boston University, Boston, MA. JAX Summer Student Program (2012).
 Virginia McLane, GSBSE, U Maine Graduate Student Rotation (2012).
 Ambreen Sayed, GSBSE, U Maine Graduate Student Rotation (2012).
 Kevin Clare, Northport High School, Long Island, NY. JAX Summer Student Program (2013).
 Jakub Dziedzic, U. Penn, Philadelphia, PA. JAX Summer Student Program (2013).
 Annie Sullivan, Red Hook HS, Red Hook, NY. JAX Summer Student Program (2014).

Ph.D. Students

Ambreen Sayed, GSBSE, University of Maine, Orono, ME. 2013-
 Paige Martin, GSBSE, University of Maine, Orono, ME. 2015-

Ph.D. – Thesis Committees

Sean M. Garvey, Duke University, Durham, NC. (PhD Awarded 2007)
 Rosemarie E. Seymour, University of Maine, Orono, ME. (PhD Awarded 2008)
 Jingxia Xu, University of Maine, Orono, ME. (PhD Awarded 2011)

Rocco Gogliotti, Northwestern University, Chicago, IL. (PhD Awarded 2012)
Ying Chen, University of Maine, Orono, ME. (PhD Awarded 2013)
Christopher Demers, GSBSE, Univ. of Maine, Orono, ME. . (PhD Awarded 2015)
Ginny McLane, University of Maine, Orono, ME.
David Maridas, University of Maine, Orono, ME.
Cong Tian, University of Maine, Orono, ME.
Leah Graham, Tufts University/JAX.
Yang Kong, GSBSE, Univ. of Maine, Orono, ME.
Emily Spaulding, GSBSE, Univ. of Maine, Orono, ME.
Kathy Morelli, GSBSE, Univ. of Maine, Orono, ME.
Sriramulu Pullagura, GSBSE, Univ. of Maine, Orono, ME.

Postdoctoral Fellows

Terry P. Maddatu, D.V.M., The Jackson Laboratory, (2001-2006).
Kimberly A. Huebsch, PhD., The Jackson Laboratory, (2003-2009).
Patricia Schroder, PhD., The Jackson Laboratory, (2007-2010).
Roger B. Sher, Ph.D., The Jackson Laboratory, (2002-2012).
Prabakaran Soundararajan, PhD., The Jackson Laboratory, (2009-2014).

Editorial and Advisory Boards:

PLoS Genetics: Associate Editor. 2007-Present.
Mouse Genome Informatics (MGI) Internal Scientific Advisory Board, TJL. 2000-Present.
GSBSE (UMaine) Graduate Admission Committee, 2012-Present
Genetic Resources Internal Scientific Advisory Board, JAX. 2010-Present.
Spinal Muscular Atrophy (SMA) Foundation. Mouse Model Advisory Committee. 2004-2005.
Nathan Shock Center of Excellence (NIA) / Jackson Aging Center Internal Scientific Advisory Board, TJL. 2005-2008.

Effect of genetic background on the dystrophic phenotype in *mdx* mice

William D. Coley^{a*}, Laurent Bogdanik^{b*}, Qing Yu^a, Jack H. van der Meulen^a, Sree Rayavarapu^a, James L. Quinn^a, Allison Saunders^b, Connor Dolan^b, Maria Candida Vila^a, Whitney Andrews^b, Catherine Lammert^b, Andrew Austin^b, Terence Partridge^a, Gregory A. Cox^b, Cathleen Lutz^{b*}, Kanneboyina Nagaraju^{a,c*}

* These authors contributed equally to the study

^a Research Center for Genetic Medicine, Children's National Medical Center, Washington, District of Columbia, United States of America

^b The Jackson Laboratory, Bar Harbor, Maine, United States of America

^c Department of Integrative Systems Biology, George Washington University School of Medicine. Washington, District of Columbia, United States of America

Abstract

Genetic background significantly affects phenotype in multiple mouse models of human diseases, including muscular dystrophy. This phenotypic variability is partly attributed to the presence of genetic modifiers that modulate the disease process. Previous studies have demonstrated that introduction of the γ -sarcoglycan null allele onto the DBA/2J background confers a more severe muscular dystrophy phenotype than in the original strain, demonstrating the presence of genetic modifier loci in the DBA/2J background. To characterize the phenotype of dystrophin deficiency on the DBA/2J background, we have created and systematically phenotyped DBA/2J-congenic *Dmd*^{mdx} mice (D2-*mdx*) and compared them to the original, C57BL/10ScSn-*Dmd*^{mdx} (B10-*mdx*) model. These two strains were also compared to their respective control mouse strains at multiple time points between 6 and 52 weeks of age. Skeletal and cardiac muscle function, inflammation, regeneration, histology and biochemistry were characterized. We found that D2-*mdx* mice showed significantly reduced skeletal muscle function as early as 7 weeks of age and reduced cardiac function by 28 weeks, suggesting that the disease phenotype is more severe than in B10-*mdx* mice. In addition, D2-*mdx* mice showed fewer central nuclei and increased calcifications in the skeletal muscle, heart, and diaphragm as early as 7 weeks of age, suggesting that their pathology is different from the one of the B10-*mdx* mice. The new D2-*mdx* model, with an earlier onset and more pronounced dystrophy phenotype may be useful for evaluating therapies that target cardiac and skeletal muscle function in dystrophin-deficient mice.

Introduction

Genetic backgrounds affect disease phenotype in both mice and in humans (1-4) (for example. A stop codon mutation within exon 23 of the mouse dystrophin gene (*Dmd*) on the X chromosome results in the absence of dystrophin (5, 6). The skeletal muscles in these mice on a C57BL/10 (B10) background (C57BL/10-*mdx* mice) undergo cycles of degeneration and regeneration, along with infiltration of immune cells and elevated levels of serum creatine kinase. As compared to B10 wild-type control mice, both male and female *mdx* mice have reduced life spans (7). These mice do not typically show significant fatty replacement or fibrosis in the skeletal muscle. However, unlike the skeletal muscle, the diaphragm in dystrophin-deficient mice undergoes extensive progressive degeneration, mineralization, and regeneration, followed by fibrosis and a loss of myofibers (8). Despite the milder phenotype in skeletal muscle, these mice are routinely used in preclinical evaluations because they are genetic and biochemical homologues of human Duchenne muscular dystrophy (DMD). In fact, the B10-*mdx* mouse is the most widely used mouse model for DMD.

Genetic mapping studies performed in Dr. Elizabeth McNally's group have shown that the introduction of the mouse sarcoglycan gamma (*Sgcg*)-null allele onto the DBA/2J genetic background confers a more severe muscular dystrophy phenotype than in the 129T2/SvEmsJ strain, demonstrating that the genetic modifier loci in the DBA/2J background affect the disease phenotype of *Sgcg*-null mice. Furthermore, this group found that polymorphism in the coding region of the latent TGF- β -binding protein 4 gene (*Ltbp4*) results in a 12-amino-acid deletion in LTBP4 that is associated with increased proteolysis, SMAD signaling, and fibrosis, suggesting that *Ltbp4* regulates TGF- β signaling and modifies the outcome in muscular dystrophy (9). Because the self-renewal efficiency of the satellite cells of DBA/2 mice is lower than that of C57BL/6 mice, Fukuda et al. generated a DBA/2-*mdx* strain by crossing DBA/2 and C57BL/10-*mdx*. They found that the hind limb muscles of DBA/2-*mdx* mice exhibited increased weakness, lower muscle weight, fewer myofibers, and increased fat and fibrosis when compared to B10-*mdx* mice, suggesting that the satellite cells' self-renewal ability may be one of reasons for the differences in pathology between these mouse strains (10).

To investigate the effect of genetic background on the dystrophic phenotype, we have created a DBA/2J-congenic DMD *mdx* (D2-*mdx* strain) mouse model. We have systematically assessed the functional, histological, biochemical, and molecular phenotype of these mice at 7, 28, and 52 weeks of age and compared them to the standard B10-*mdx* and the two respective background control strains (DBA/2 and C57BL/10). Some of the parameters were assessed and reproduced in two different laboratories (the Children's National Medical Center [CNMC] and The Jackson Laboratory) in independent cohorts of mice. We found that D2-*mdx* mice showed significantly reduced cardiac and skeletal muscle function, suggesting that genetic background significantly affects the disease phenotype of dystrophic mice.

Results

Body weight: The body weights for mice were measured at 7, 28, and 52 weeks of age (Supplemental Tables 1). We compared body weights recorded at the 28-week time point at both the CNMC (Fig.1A) and The Jackson Laboratory (Fig.1B). We found that B10-*mdx* mice were generally bigger than the B10 controls, whereas the D2-*mdx* mice were significantly

smaller than the DBA/2 control mice. The two wild-type strains (B10 and D2) were not significantly different from each other at this age, whereas D2-*mdx* mice were significantly smaller than the B10-*mdx* mice. The differences in the body weights between the *mdx* and wild-type strains were consistent between the two laboratories (Fig.1A and B).

Tissue weights: We examined the weights of the gastrocnemius, tibialis anterior (TA), and quadriceps muscles and the heart and spleen tissues in all strains (Supplemental Tables 1). We found that the muscle weights of the two control strains were the most similar. For all three muscles, the B10-*mdx* mice showed an increase in muscle mass. In contrast, D2-*mdx* mice showed a loss of muscle mass in all three muscles at all time points when compared to the D2 mice. The muscle/body weight ratios for many muscles were lower in the D2-*mdx* than in D2 mice from the 28th week on, suggesting a muscle atrophy, while the muscle/body weight ratios in B10-*mdx* were higher than in B10 mice, reflecting the well-documented muscle hypertrophy of this model. We also found that the mass of the heart differed significantly between the two control strains. The mass of the heart did not differ between strains at 7 weeks of age, but with age, the D2 hearts became significantly larger than the B10 hearts. This increase in cardiac mass was mirrored in the D2-*mdx* mice, whose hearts were similar in size to those of the D2 strain. However, the B10-*mdx* mice were also observed to have enlarged hearts, relative to the B10 controls, although this enlargement was significant only at the last time point.

Fiber diameter measurement: To determine the effect of genetic background on muscle fiber diameter, we evaluated the average diameter of the muscle fibers in the TA muscle. Cross-sections of the fixed TA muscle were stained for reticulin in order to clearly mark muscle fiber surfaces. Representative images of reticulin staining are shown in Fig. 2A. We found that the average fiber diameters were shifted in opposite directions by the *mdx* mutation, depending on the background strain. B10-*mdx* mice were found to have fewer normal-sized fibers (500-2000 pixels across) and a greater proportion of hypertrophic fibers (2000+ pixels) (Fig. 2B). This observation is consistent with prior findings of hypertrophy in this strain (11). In contrast, the D2-*mdx* mice were found to have relatively few hypertrophic fibers alongside a large number of small fibers. Specifically, the average fiber diameter was reduced to 500 pixels across, from the average of 1000 pixels seen in control DBA/2 mice. These results are consistent with our findings regarding changes in muscle mass and muscle/body weight ratios between the two strains.

Creatine kinase enzyme activity: Serum CK enzyme activity was determined at 28 weeks of age by both the CNMC (Fig. 3A) and The Jackson Laboratory (Fig. 3B). The two control strains (B10 and D2) were both found to have minimal amounts of CK activity. Both *mdx* mutant strains were observed to have significantly elevated levels of serum CK activity when compared to age-matched controls. D2-*mdx* mice showed relatively lower serum CK levels than did the B10-*mdx* mice at 24 weeks of age. The serum CK data were consistent between the two laboratories.

Evans blue dye uptake: Damage to muscle fibers can also be measured by quantifying the uptake of Evans blue dye (EBD) by the muscle tissue. Trapped EBD can either be visualized via fluoroscopy in fixed tissues (Fig. 4A-D) or quantified in muscle lysates via spectroscopy (Fig. 4E). The quantification of EBD retained within these tissues confirmed that the two *mdx* strains had significant uptake when compared to their respective controls. However, the D2-*mdx* mice were found to have a significantly higher uptake of EBD than did the B10-*mdx* mice.

Grip strength: The grip strength measure (GSM) for all four-mouse strains was performed at both the CNMC and the Jackson Laboratory. At CNMC, GSM was measured at 28 and 52 weeks of age in the forelimbs and hindlimbs, and at The Jackson laboratory in the forelimbs at

6, 12, and 24 weeks of age (Sup. Fig.1). Because of the differences in the body weights of the different strains, the forelimb and hindlimb maximal force (kgf) data were normalized to the body weight of the animal and are presented as normalized grip force (kgf/kg). There was an overall decline in grip strength in all strains by 52 weeks of age (Sup. Fig.1). *mdx* mice on both backgrounds showed significantly lower normalized grip strength than did their respective control mouse strains in both laboratories at the 24 or 28-week time points (Fig.5A and B). The normalized GSM data for the hindlimbs collected at the CNMC were consistent with the forelimb data collected at both laboratories.

In vitro EDL force contraction: The weights of the EDL muscles showed that the D2 mice had significantly smaller EDL muscles than did the BL10 mice at 7 weeks of age, and these differences were reduced at the 28-week and 52-week time points. B10-*mdx* mice showed significantly more muscle mass than did control BL10 mice at 28 and 52 weeks of age, whereas D2-*mdx* mice showed a lower EDL mass than did the control D2 mice at 28 and 52 weeks of age (Fig. 6A).

We then evaluated the maximal force and specific force production of the EDL muscles but did not detect any significant differences in either the maximal or specific force between the two wild-type control strains at any time point. The maximal force shown by the EDL muscles of the BL10-*mdx* mice was similar to that of the BL10 controls at all time points (Fig. 6B). In contrast, the specific force significantly decreased at all time points in the BL10-*mdx* mice when compared to the BL10 controls (Fig. 6C). Unlike the BL10-*mdx* mice, the D2-*mdx* mice showed a significant reduction in both maximal and specific force at all three time points tested (Fig. 6B and C).

Echocardiography and cardiac function: The assessment of heart function was carried out using echocardiography on live, sedated mice. We found that the ejection fraction (EF) and shortening fractions (SF) were significantly higher at 7 weeks of age in the wild-type D2 mice than in the wild-type BL10 mice; however, these differences were lost at 28 and 52 weeks of age. The D2-*mdx* mice showed a significantly lower EF and SF than did the control D2 strain, whereas the EF and SF values for the BL10-*mdx* and BL10 mice were similar at 28 weeks of age (Fig. 7 A and B). By 52 weeks of age, both strains showed significant deficits in EF and SF when compared to their respective wild-type strains. We also found a significant drop in stroke volume (Sup. Fig. 2A), and cardiac output (Sup. Fig. 2B) in both strains when compared to their wild-type controls.

Histological (H&E) evaluation of muscle tissues: We examined the diaphragm, quadriceps, and heart muscles for muscle damage at 7, 28, and 52 weeks of age. Representative images for the diaphragm (Fig. 8A), heart (Fig. 8B), and quadriceps (Sup. Fig. 3) are shown for all four strains at all three time points. The histologic appearance of all three tissues was normal for the control BL10 and D2 strains at all time points. At 7 weeks, both *mdx* strains showed lesions exhibiting muscle degeneration, regeneration, and mononuclear infiltrating cells within the quadriceps and diaphragm. In addition, the D2-*mdx* mice, but not the B10-*mdx* mice, showed significant calcification in all tissues. We also observed that the D2-*mdx* mice showed signs of inflammation within the cardiac tissue at 7 weeks of age, whereas the B10-*mdx* mice showed normal cardiac histology at that age.

To quantify the calcified deposits, we performed microCT scanning (Sup. Fig. 4A-4C) and found that calcified deposits were distributed throughout the muscle tissue in the quadriceps and diaphragm and in the epicardium of the heart tissue. Overall, a significant increase in tissue density as early as 7 weeks was seen only in the D2-*mdx* mice (Sup. Fig. 4D-4F).

Optical imaging to monitor muscle inflammation: We have previously demonstrated that optical imaging of Cathepsin B (CTSB) activity in live mice using cathepsin caged near-infrared imaging is an ideal method to sensitively monitor inflammation and regeneration in dystrophic skeletal muscle (12). We evaluated cathepsin activity in all mouse strains at 7 and 52 weeks of age (Sup. Fig 5) and found that cathepsin activity in the forelimb was similar between wild-type strains at both ages whereas hind limb cathepsin activity was higher in D2 mice at 7 weeks and decreases significantly at 52 weeks in comparison to BL10 mice. Both BL10-*mdx* and D2-*mdx* mice show highly significant elevation of cathepsin activity in both fore and hindlimbs at 7 weeks in comparison to wild-type control strains. D2-*mdx* but not BL10-*mdx* mice show significantly increased cathepsin activity at 52 weeks of age in comparison to their respective controls. The differences in cathepsin activity between the strains are less marked at 52 weeks of age (Fig.9A and B).

QRT-PCR of inflammatory genes: To determine whether the components of the inflammatory process differed between the B10-*mdx* and D2-*mdx* mice, we analyzed the relative gene expression of 14 different inflammation-related transcripts in all four strains of mice. This QRT-PCR procedure was performed at CNMC using mRNA isolated from the TA muscle taken at the 7-week and 52-week time points. Similar QRT-PCR analyses were carried out at the Jackson Laboratory at the 12-week time point. In general, the results from both labs confirmed that there were significant differences between the two *mdx* strains. Figure 10 shows the change in relative expression over time for a select few of the assayed genes. A complete table of the QRT-PCR results from both laboratories is provided in Supplemental Table 2. Pro-inflammatory cytokines such as TNF-alpha were consistently elevated at both time points in the *mdx* strains when compared to their wild-type controls, whereas other pro-inflammatory cytokines such as IL-6 and IL-1-beta were increased at 52 weeks of age in both *mdx* strains when compared to their controls (Fig.10). These two cytokines were significantly higher in the D2-*mdx* mice than in the B10-*mdx* mice. Some markers of macrophage migration (CCL2 and EMR1) were highly upregulated in both strains early in the disease and showed a significant decrease in old age. Type 1IFNb was expressed to a greater extent in the control strains than in the *mdx* mouse strains.

Central nuclei and BRDU labeling: Central nucleated fibers are markers of muscle regeneration. Using H&E stained sections, we quantified the percentage of centrally nucleated fibers in cross-sections of B10-*mdx* and D2-*mdx* skeletal muscle (Fig. 11A and B). Both *mdx* strains showed significantly higher numbers of centrally nucleated fibers than in their respective wild-type strains, but the D2-*mdx* mice showed significantly fewer centrally nucleated fibers than did the B10-*mdx* mice (Fig. 11E).

To evaluate whether the turnover of myonuclei differs between the two *mdx* mouse strains, we treated mice with bromodeoxyuridine (BRDU) in their drinking water. BRDU is a nucleotide analogue that is incorporated into newly synthesized DNA and can later be visualized by immunohistochemical staining. Representative images of BRDU-labeled nuclei from B10-*mdx* and D2-*mdx* TA muscles are shown in Fig. 11C and D. A comparison of BRDU⁺ nuclei between the two *mdx* strains revealed that they had similar total numbers of BRDU⁺ cells (Fig. 11F), but that the D2-*mdx* mice showed significantly fewer central BRDU⁺ nuclei than did the B10-*mdx* mice (Fig. 11G).

Myosin heavy chain expression: Muscle fibers express various homologues of the myosin heavy chain protein at various stages of development or repair. Embryonic and neonatal myosin genes (*Myh3* and *Myh8*, respectively) are markers for muscle fiber regeneration when they are expressed in adult muscles (13). Differential myosin expression can also be used to distinguish

various muscle fiber types as fast type IIA (*Myh2*), fast type IIB (*Myh4*), or slow type (*Myh7*). Slow muscle fibers express higher levels of utrophin and have an increased mitochondrial respiration, both of which have been proposed as mitigating factors in DMD(14, 15). Therefore, we tested the hypothesis that the severe pathology seen in the D2-*mdx* mice could be explained by a lack of either regenerating or slow-type muscle fibers.

Myosin expression was quantified at the RNA level in the all four mouse strains at the 8-week time point (Fig. 11H). As expected, the two healthy background strains showed low levels of expression of *Myh3* and *Myh8* (markers for regeneration) when compared to the *mdx* mutant strains. The significantly elevated ($p<0.001$) levels of *Myh3* and *Myh8* seen in B10-*mdx* mice are consistent with prior reports(16), and the D2-*mdx* strain had similarly high levels of *Myh3* and *Myh8* expression. Both the healthy DBA/2 and mutant D2-*mdx* strains were observed to have significantly higher ($p<0.01$) basal levels of *Myh7* expression than did the control B10 and mutant B10-*mdx* strains. There were no differences in *Myh4*, *Myh2* or *Myh7* expression for either strain.

Discussion

It is well known that the phenotype of a given single-gene mutation in mice is modulated by the genetic background of the inbred mouse strain in which the mutation is maintained. This effect is attributable to modifier genes, which function in combination with the causative gene. Developing congenic mouse strains not only helps us to investigate the effect of genetic background on phenotype but would also facilitate the development of mouse models that more accurately mimic certain features of human disease (17). The commonly used *mdx* mouse models for DMD are on the C57BL/10ScSn background. In these mice, the disease progression in skeletal muscle (with the exception of the diaphragm) is mild when compared to the disease progression in humans. It has previously been shown that transfer of the γ -sarcoglycan null allele and the *mdx* mutation onto the DBA/2J background confers a more severe muscular dystrophy phenotype (9, 10). Therefore, we decided to generate congenic mice carrying the *mdx* 23 mutation on the DBA2/J background. In this paper, we report that *mdx* mice on the DBA2/J genetic background have more skeletal muscle damage and inflammation, as well as an early onset of cardiac disease when compared to *mdx* mice that are on the C57BL/10ScSn background.

Systematic phenotyping of these mice in two different laboratories has revealed consistent and reproducible data. We measured body weights at three ages and tissue weights at the end of the study and found that the body weights did not differ significantly between the two strains of wild-type mice, but the two *mdx* mouse strains showed opposite effects in terms of body weight. The B10-*mdx* mice were generally heavier than the B10 controls, suggesting that there some degree of hypertrophy had occurred in the mutant strain. BL10 and B10-*mdx* muscles generally attained maximum size by 12 to 14 weeks, at which point the B10-*mdx* muscle fibers were up to 50% larger than those of the B10 mice (18). Conversely, the D2-*mdx* mice were much smaller than those of the control DBA2 strain, suggesting an atrophic phenotype. Our observations are consistent a previous report that has shown a significant difference in muscle weight per body weight between D2-*mdx* and control littermates (10). Our study also demonstrates that the decrease in body weight is associated with significant decreases in the gastrocnemius, TA, and quadriceps muscles. The differences in muscle mass were also observed in the sarcoglycan-null mice with a DBA/2 background (10), suggesting that

genetic background has an influence on body weight and muscle mass. Evaluation of the muscle fiber diameter of TA muscles suggested that a significantly higher number of smaller fibers were present in the D2-*mdx* mice; thus, the differences in muscle mass are apparently also reflected at the level of the muscle fiber diameters.

We next evaluated whether any of the muscle injury markers were significantly different in the two *mdx* mouse strains, by quantitating serum CK levels as well as EBD dye uptake into skeletal muscle. We found significantly increased serum CK levels in both strains when compared to their respective control strains. The serum CK levels were slightly lower in the D2-*mdx* mice than in the B10-*mdx* mice, suggesting that atrophy and a loss of muscle mass had occurred in both mutant strains, but to a slightly greater extent in the D2-*mdx* mice than in the B10-*mdx* mice. On the other hand, EBD dye uptake was significantly higher in the D2-*mdx* mice than in the B10-*mdx* mice, suggesting that an increased number of leaky necrotic muscle fibers were present in both mutant strains, particularly in the case of the D2-*mdx* mice. These data contradict previous findings that have shown fewer total necrotic fibers in D2-*mdx* mice (10). These differences could be a result of the different methodologies used for EBD quantitation (spectrometric evaluations vs. counting of EBD-positive muscle fibers).

To evaluate the effect of genetic background on muscle function, we performed grip strength measurements and also measured the in vitro force contractions of the EDL muscle. We found that forelimb grip strength was significantly reduced in both *mdx* mouse strains at 28 weeks of age. A previous study by Fukada et al., 2010 reported differences in grip strength between D2-*mdx* and their congenic controls, but not between B10-*mdx* and B10 control mice (10). It is pertinent to note that our grip strength assessments were done in two independent groups of mice by two different laboratories. Since grip strength is subjected to an animal's volition, we also performed in vitro force measures on isolated EDL muscles. The EDL muscle mass of D2-*mdx* mice was, on average, much smaller than that of the B10-*mdx* mice; the maximal force generated by the B10-*mdx* mice was equal to that of both wild-type strains. Thus, the maximal force data obtained for both the BL10 and B10-*mdx* mice was consistent with previous data reported in the literature (19). In contrast, the specific force in both *mdx* strains was much lower than that of the respective control strains; however, the D2-*mdx* mice generated a significantly lower force than did the B10-*mdx* mice, suggesting that the muscle damage is more severe in the D2-*mdx* mice. Interestingly, the specific force deficit stayed relatively constant and did not change with age in either *mdx* mouse strain. This force deficit was consistent with our histological findings indicating that D2-*mdx* muscle tissue shows a more pronounced muscle pathology does that of B10- *mdx* mice.

Since muscle inflammation is a major component of the disease pathogenesis in dystrophin deficiency, we previously developed a method for detecting inflammation in live animals by using optical imaging of cathepsin B (CTSB) activity. This sensitive method for monitoring inflammation uses a caged near-infrared CTSB substrate, ProSense 680 (12). Using this method, we have now demonstrated that the CTSB activity is highest in both *mdx* strains at 7 weeks of age and decreases significantly by 52 weeks of age, suggesting that inflammation plays an important role early in the disease process in both of these mouse models. This trend in cathepsin activity is likely related to the infiltration of macrophages (a major source of cathepsin release) (20). Indeed, we measured a very strong increase in mRNA markers of macrophages (*Lgals3* and *Mpeg1*) in the muscle of the *mdx* mice, and this increase was more

pronounced in the D2 background. These data are also consistent with our previous study in which we found stage-specific remodeling of human dystrophin-deficient muscle, with inflammatory pathways predominating in the early stages and acute activation of TGF-beta and failure of metabolic pathways later in the disease (21). We also found that the early increase and gradual drop in inflammation is reflected in the pro-inflammatory cytokine expression in skeletal muscle (22). Cytokines are differentially expressed in the wild-type strains (both backgrounds). Furthermore, it is known that the DBA/2 strain has an in-frame deletion within the LTBP4 gene that confers a severe disease phenotype, and it has been proposed that its pathogenic effects are mediated by excessive TGF β signaling. Intriguingly, a polymorphism in LTBP4 has also been implicated in the pathogenesis of DMD (23).

The self-renewal efficiency of satellite cells after muscle injury in the DBA/2 mouse strain has been shown to be lower than that of C57BL/6 mice (10). Therefore, we evaluated the percentage of central nuclei (%CNF), BRDU dye uptake, and myosin heavy chain subtypes in our four mouse strains. We found that the %CNF as well as the number of BRDU-positive central nuclei was significantly lower in the D2-*mdx* mice than in the B10-*mdx* mice, suggesting that there is a lower regeneration and turnover of myonuclei in the D2-*mdx* mice. These differences were not reflected at the level of *Myh3* and *Myh8* transcript expression. Unlike the B10-*mdx* mice, we found that the D2-*mdx* mice showed enhanced calcification in their skeletal muscle, diaphragms, and heart tissue. This enhanced calcification could be strain-specific, because dystrophic cardiac calcifications are often found in DBA/2 mice, reportedly in association with low plasma magnesium levels (24).

We have previously shown that heart dysfunction in B10-*mdx* mice is prominent at 9-10 months of age and is associated with a significantly increased LV internal diameter (at end systole) and a decreased posterior wall thickness. This cardiomyopathy is associated with a 30% decrease in shortening fraction (25). Our current evaluations of cardiac function now reveal that the D2-*mdx* mice show early cardiomyopathy by 28 weeks, considerably earlier than their B10-*mdx* counterparts. These echocardiography results were also consistent with our histological findings. Specifically, we observed cardiac tissue inflammation and damage in D2-*mdx* mice as early as 7 weeks of age, and this damage became progressively worse over time. In contrast, the B10-*mdx* mice did not show any histological signs of cardiomyopathy until 28 weeks, and functional deficits on echocardiography were not seen until the testing at the 52-week time point.

In summary, our data suggest that D2-*mdx* mice have severe progressive muscle disease with early-onset cardiac deficits. The muscle hypertrophy response that is predominant in the B10-*mdx* model and complicates the study of muscle wasting in this strain, is notably absent in the D2-*mdx* model. Thus, this mouse model may be a particularly suitable model for evaluating therapeutics for DMD.

Materials and Methods

Animal Husbandry

Animals were housed at a density of up to 5 males or 5 females per cage under specific pathogen-free conditions in rooms with a 12-h light/12-h dark cycle at a temperature of 18–23°C and 40–60% humidity. At the CNMC, all mice were handled according the local guidelines established by the Institutional Animal Care and Use Committee (IACUC) of the CNMC in

Washington D.C., and all procedures were carried out under the approved animal protocol. At The Jackson Laboratory, all experiments were conducted in accordance with the protocols described by the National Institutes of Health's Guide for the Care and Use of Animals and were approved by The Laboratory's institutional animal care and use committee. The wild-type strains C57BL/10 (JAX Stock #000476 and #000665; B10) and DBA/2 (JAX Stock #000671; D2) served as the genetic background controls for the two mutant strains C57BL/10ScSn-*Dmd*^{mdx} (JAX Stock #001801; B10-*mdx*) and D2.B10-Dmd^{mdx}/J (JAX Stock #013141; D2-*mdx*), respectively. Control mice at CNMC were descended from stock #000476, and the equivalent controls at The Jackson Laboratory were drawn from stock #000665. Only males were used for this project.

Genotyping

The DBA2 mouse strain has been reported to have a mutation in the LTBP4 gene that may affect muscle function and regeneration (9). Genotyping for this reported deletion mutation was carried out by standard PCR, followed by gel electrophoresis. The product size of the wild-type LTBP4 band is 273 bp, whereas the band for the mutant is only 236 bp. The primers used to identify the LTBP4 status are listed in Table 1. Genotyping of the MDX exon 23 SNP was performed via real-time allelic discrimination using custom-made Taqman® fluorescent-bound primers. SNP genotyping reactions were conducted using the Taqman® SNP Genotyping Master Mix according to the manufacturer's recommendations. The primers used to identify the MDX23 SNP are listed in Table 1:

Table 1: Primers used for genotyping

Primer Name	Dye Conjugate	Sequence
LTBP4 Forward	n/a	ctgggccacagcctgaac
LTBP4 Reverse	n/a	aagcctttccccacagaaat
MDX23 Forward	n/a	tgaggctctgcaaagttcttgaa
MDX23 Reverse	n/a	catctccttcacagtgtcactca
MDX23 Wild type	VIC	aagccattttgttgctct
MDX23 Mutant	FAM	aagccattttattgctct

Functional and behavioral activities

CNMC Grip strength test: Grip strength for both fore- and hindlimbs was assessed using a grip strength meter consisting of a horizontal forelimb mesh and an angled hind limb mesh (Columbus Instruments, Columbus, OH) according to a previously published protocol(22). The animals were acclimatized on fore- and hindlimb meshes for 3 consecutive days prior to data collection, and then for 90 sec before actual data collection began. Force was measured according to the amount of horizontal force that was required to break the mouse's grip from the mesh surface. Five successful hindlimb and forelimb strength measurements were recorded within 2 min. The maximum values of each day over a 5-day period were averaged and normalized to body weight and expressed as KGF/kg unit.

CNMC behavioral activity testing: Voluntary activity in an open field was measured using an open-field Digi-Scan apparatus (Omnitech Electronics, Columbus, OH) as described previously (22). All mice were acclimatized to the scanning chamber one week prior to actual data

collection. The data were collected every 10 min over a 1-hr period each day for 4 consecutive days. The results were calculated as mean \pm standard error for all recordings. The recorded quantitative measures of activity were horizontal activity, vertical activity, total distance, and rest time.

CNMC Rotarod testing: The latency-to-fall from the Rotarod apparatus was assessed as described previously (22). In brief, mice were trained on the Rotarod (Ugo Basile, Italy) for 2 days before data collection was begun. Each trial consisted of placing the mouse on the rod at 10 rpm for 60 sec (stabilizing period), followed by acceleration from 10 rpm to 40 rpm. Each trial was done twice a day for 3 consecutive days, with a minimum 2-hr interval between the data collection times. The latency-to-fall was recorded, and average values were calculated from all six scores.

Jackson Laboratory grip strength measurements: The strength exerted by the forelimbs of an animal in response to a constant horizontal force was measured. The grip-strength meter (Chatillon-Ametek Digital Force Gauge, DFIS 2, Columbus Instruments, Columbus, OH) was positioned horizontally, with the triangular metal transducer situated 10 cm above a foam platform. Each mouse was raised toward the triangular transducer, and it instinctively grasped for the bar. Care was taken to ensure the mouse was holding the grip transducer properly with, and only with, both front paws. Once an appropriate grip was observed, the animal was pulled horizontally from the bar. Peak force was measured in kg for 5 consecutive trials per mouse. The maximum force was retained for each animal. For the fatigue quantification, force at the fifth trial was expressed as a percentage of the force at the first trial. Forces were normalized to body weight.

Jackson Laboratory behavioral activity measurements: Voluntary activity measurement consisted of recording 30 min of the horizontal and vertical (rearing) activities in an open field (BiObserve, Germany) for each mouse. Mice were all tested in the morning (9-11 am).

Force contractions on isolated skeletal muscle

Force contraction experiments were conducted on the EDL muscle of the right hindlimb of each mouse. The mouse was anesthetized with an intraperitoneal injection containing ketamine (100 mg/kg) and xylazine (10 mg/kg). The muscles were isolated, and 6-0 silk sutures were tied securely to the distal and proximal tendons. Each muscle was then carefully removed from the mouse and placed vertically in a bath containing buffered mammalian Ringer's solution (137 mM NaCl, 24 mM NaHCO₃, 11 mM glucose, 5 mM KCl, 2 mM CaCl₂, 1 mM MgSO₄, 1 mM NaH₂PO₄, and 0.025 mM tubocurarine chloride) maintained at 25°C and bubbled with 95% O₂-5% CO₂ to stabilize the pH at 7.4. The distal tendon of the muscle was tied securely to the lever arm of a servomotor/force transducer (model 305B, Aurora Scientific) and the proximal tendon to a stationary post in the bath. After removal of the muscle, the mouse was euthanized by gassing with CO₂ according to IACUC guidelines. The muscle was stimulated between two stainless steel plate electrodes. The voltage of single 0.2-msec square stimulation pulses was increased until supramaximal stimulation of the muscle was achieved, and the muscle length was then adjusted to the length that resulted in maximal twitch force (i.e., optimal length for force generation). With the muscle held at optimal length, the force developed during trains of stimulation pulses was recorded, and stimulation frequency was increased till the maximal isometric tetanic force was achieved. For the EDL muscle, 300 ms trains of pulses were used,

and a stimulus frequency of ~220Hz was typically needed to achieve the maximum isometric force. The muscle length was measured with calipers, and the optimal fiber length was calculated by multiplying the optimal muscle length by a constant of 0.45, an established fiber length/muscle length ratio for EDL muscle.. The muscle mass was determined after removal of the muscle from the bath. The muscle-specific force, a measure of the intrinsic force generation of the muscle, was calculated according the following equation: specific force = maximal isometric force/ (muscle mass * (density of muscle tissue * fiber length)⁻¹). The muscle tissue density was 1.056 kg/L.

Echocardiography

In order to assess the cardiac function of mice *in vivo*, we performed echocardiography on sedated mice. Mice were first anesthetized with 5% isoflurane mixed with 100% oxygen at 1.0 L/min flow, then maintained under anesthesia with 1.5% isoflurane/oxygen flow. Ophthalmic ointment was placed on the eyes to prevent drying of the cornea while the mouse was anesthetized and tested. After anesthetic induction the animals, were placed on a thermostatically controlled heated platform, where isoflurane anesthesia was maintained by delivery through a close fitting face-mask. A heating lamp was also used to keep the heart rate and body temperature constant at physiological status during echocardiography. During the examination, the animal's heart rate was monitored through the use of an electrocardiograph. The mouse's heart rate and body temperature were monitored continuously during the scanning. Fur was removed from the ventral surface of the mouse torso with clippers and Nair (Church & Dwight, Ewing, NJ). Echocardiography was performed using Vevo770 ultrasound machine (VisualSonics, Toronto, Canada). The 2-D (B-mode), M-mode, and Doppler images were acquired from a modified parasternal long axis view, parasternal short axis view, suprasternal notch view, and apical three-chamber view. The heart rate (BPM), fractional shortening (FS), ejection fraction (EF), stroke volume (SV), and cardiac output were obtained for cardiac function assessment using measurements from the modified parasternal short axis view in the M-mode. Qualitative and quantitative measurements were recorded using Veto 770 offline workstation software, and post-imaging analysis was performed using the VevoStrain analytic software.

Optical Imaging

Cathepsin enzyme activity is used as a marker for inflammation, and this activity can be detected *in vivo* by detecting the cathepsin-mediated cleavage of certain dye molecules. Mice were prepared for optical imaging by administering an intraperitoneal injection of 1.5 nmol of ProSense 680 (VisEn Medical), prepared in a total volume of 150 µl, 24 h prior to imaging. One the day of the imaging, mice were sedated using 1.5-2% isoflurane and 100% oxygen before being placed inside the eXplore Optix (GE Healthcare) scanning chamber. The floor of the scanning chamber was continuously heated to maintain normal body temperature. Nair (Church & Dwight, Ewing, NJ) was used to remove fur from the limbs prior to scanning. The scan plane was kept consistent between the mice, at a height that was immediately above the hindlimbs. The scanning area was limited to the limbs. For scanning, a 670-nm excitation frequency was used with a 1.0 mm resolution. Emissions were collected using a 700-nM long-pass filter. The acquired photon intensity data was automatically normalized by the Optiview 2.0 software to

account for differences in scanning laser power and integration times selected between mice. The measured cathepsin activity was defined as photon intensity (photon counts/mm²).

MicroCT scan

The tissue density of formalin-fixed tissues was determined by a MicroCT scan. MicroCT analysis was performed on fixed gastrocnemius, quadriceps, heart, and diaphragm tissues using a SkyScan 1172 MicroCT (Bruker, Belgium). Imaging was performed at a 40-kV source voltage, 250- μ A source current, 295-ms exposure time, and 0.4° rotation step, with a 0.5-mm aluminum filter. The imaging resolution size was 9 μ m. Three-dimensional reconstructions were performed with Skyscan NRecon and Dataviewer software. For analysis, tissues were selected individually for a polygonal region of interest within the whole tissue area. Tissue density data were obtained from 3D analysis of the selected tissues using Skyscan CT-analyzer software.

Serum creatine kinase activity

At CNMC, blood was collected from mice via cardiac puncture immediately following sacrifice. Serum was separated from other blood fractions by centrifugation and stored at -80°C without EDTA or heparin. CK activity in the serum was measured using the Creatine Kinase Reagent Set from Pointe Scientific, Inc. (Canton, MI) according to the manufacturer's protocol. In brief, 25 μ l of serum was pipetted into a volume of pre-warmed detection reagent in a 96-well plate and allowed to incubate for 2 min at 37°C. The absorbance of each well on the plate was then read once per min for 5 min. The average change in absorbance was then used to calculate the concentration of CK in U/L, where one U was defined as the amount of CK required to catalyze the conversion of one micromole of creatine phosphate in 1 min at 37°C. All measurements were made on a BioRad xMark spectrophotometer at 340 nm at 37°C using a standard clear 96-well plate. At The Jackson Laboratory, blood was collected by retro-orbital sinus puncture into heparinized glass capillaries, immediately after the last test. Serum was isolated by centrifugation for 10 min at 14,000 rpm. Creatine kinase (CK) was measured with a Beckman Coulter AU Clinical Chemistry analyzer.

Histology

H&E staining: Freshly dissected tissues were prepared for histology by fixing tissues with 0.4% neutral buffered formalin (Fisher Scientific) sealed in glass scintillation vials (Fisher Scientific). Fixed tissues were then sent to Hisotserv Inc. (Germantown, MD) to be mounted in paraffin wax, sectioned, and stained with hematoxylin and eosin (H&E). Tissue sections stained with H&E were imaged using an Olympus BX51 microscope with attached Olympus DP70 camera module.

Immunofluorescent staining

Immunofluorescent staining for utrophin and neonatal myosin was performed on gastrocnemius, tibialis anterior, and diaphragm cryosections using the antibodies VP-U579 (Vector Laboratories) and ab49457 (Abcam), respectively. An AlexaFluor® 488-goat anti-mouse IgG1 antibody (Life Technologies) was used as a secondary antibody. Confocal (TCS SP5, Leica) images were acquired at 20x magnification, and the number of positive fibers per microscope field was counted. Counts from three fields were averaged for each muscle.

BRDU staining

Frozen muscle tissues were mounted in Optimal Cutting Temperature compound (Tissue-Tek) and cut on a microtome to produce 8 μ m-thick cross-sections. For bromodeoxyuridine (BRDU) staining in muscle sections, sections were first allowed to air dry for 5 min before being fixed with HCl. The fixation procedure involved washing slides in Tris-buffered saline + 0.1% Tween-20 (TBST), then submerging them in acetone (pre-chilled to -20°C) for 10 min, followed by a second wash in TBST for 5 min. Fixed slides were then incubated in 2N HCl for 1 hour at 37°C, followed by neutralization with 0.15 M sodium borate (pH 8.5) for 10 min at room temperature. Next, slides were washed with TBST and then incubated in blocking buffer (2% BSA, 5% normal goat serum, 0.5% Triton-X100, and 0.1% Tween-20 in PBS) for 1 h at room temperature. Antibody buffer was made by diluting the blocking buffer 1:10 with PBS. Blocked slides were washed in PBS, then incubated with primary biotinylated anti-BRDU antibody ([#B35138, Life Technologies] diluted 1:125 in antibody buffer and primary anti-laminin ([#L9393, Sigma-Aldrich] diluted 1:125 in antibody buffer) overnight at 4°C. Slides were then washed in PBS before incubation with streptavidin-FITC secondary antibody ([#434311, Life Technologies] diluted 1:600 in antibody buffer) and anti-rabbit Alexafluor-594 ([#A11012, Life Technologies] diluted 1:600 in antibody buffer) for 1 h at room temp. Images were captured using an Olympus BX61 microscope with attached Olympus DP71 camera module. Counting was performed in a blinded fashion using whole cross-sections of the TA muscle, with 3 whole cross-sections per group.

Evan blue dye (EBD) uptake

EBD uptake by the gastrocnemius was quantified as described previously (26) with minor modifications. EBD (Sigma, E2129) was dissolved in PBS at 10 mg/ml. Each animal received an intraperitoneal injection at 5 μ l/g body weight; 24 hours after the injection, the gastrocnemius muscles were harvested, homogenized, and incubated at 55°C in 1 ml formamide for 2 h. The suspension was cleared by centrifugation at 6,000 g for 5 min, and spectrophotometric absorbance was measured at 620 nm on the cleared lysate. Protein concentration was determined by BCA assay (Pierce, catalog # 23225). Results were recorded as absorbance/ μ g of tissue.

Myosin heavy chain identification

For the myosin isoform quantification, assays were performed for the following: myosin 3 (embryonic) (PrimerBank ID 153792648c1), myosin 8 (neonatal) (PrimerBank ID 28893527a1), myosin 7 (slow) (PrimerBank ID 118131045c1), myosin 4 (fast IIB) (PrimerBank ID 67189166c1), and myosin 2 (fast IIA) (PrimerBank ID 205830427c1). All assays were performed using the SYBR® Green method (Life Technologies) on a ViiA™ 7 Real Time PCR System (Life Technologies). GAPDH (PrimerBank ID 126012538c1) was used as a reference gene. Utrophin RNA quantification was performed with the Mm01168866_m1 TaqMan Gene Expression Assay (Life Technologies) multiplexed with GAPDH. Fold changes in expression were calculated by using the average $\Delta\Delta$ Ct for the gene of interest in the control B10 group as the reference. Statistical analysis consisted of a two-way ANOVA followed by a Tukey's multicomparison test performed on the $\Delta\Delta$ Ct values.

Fiber size measurement and nuclear counting

After dissection, the hindlimbs were fixed in 2% paraformaldehyde in PBS overnight at 4°C. The tibialis anterior was then dissected and paraffin-embedded. Five micron-thick microtome cross-sections were cut at the level of the belly of the muscle and stained for reticulin: Slides were deparaffinized and hydrated, oxidized in 1% potassium permanganate, bleached in 1% oxalic acid, sensitized in 2.5% ferric ammonium sulfate, impregnated with freshly prepared working silver solution (10% silver nitrate, sodium hydroxide and ammonium hydroxide), toned in 0.2% gold chloride solution, placed in 5% sodium thiosulfate, dehydrated, cleared, and mounted. Slides were scanned at a 20x magnification on a digital slide scanner (NanoZoomer 2.0HT, Hamamatsu). A region of interest was drawn on the ventral side of the muscle and analyzed with ImageJ, using the Threshold and Analyze Particle functions, to return the number of fibers and their individual cross-sectional areas. An average of 400 fibers was measured per muscle. Fiber size repartition was drawn using a 50-pixel binning. The percentage of fibers with centrally located nuclei was counted manually on the same regions of interest.

Inflammatory marker detection

Jackson Laboratory RT-QPCR: Total RNAs were extracted from the TA muscle using the Trizol method, and 800 ng of total RNAs were treated with DNase and reverse-transcribed, with 40 ng of cDNA used per 10- μ L quantitative PCR reaction. For the Jackson Laboratory inflammation marker panel, the following assays were selected from the PrimerBank website ((Spandidos et al., 2010), <http://pga.mgh.harvard.edu/primerbank/>): TNF-alpha (PrimerBank ID 133892368c1), interleukin-6 (PrimerBank ID 13624310c1), Mpeg1 (PrimerBank ID 133506752c1), Lgals3 (PrimerBank ID 225543162c1), CD53 (PrimerBank ID 161484612c1), CD48 (PrimerBank ID 145966847c1), Lyc6c1 (PrimerBank ID 26353880a1), LTB (PrimerBank ID 161760676c1), and CD11b (PrimerBank ID 132626288c1).

For the CNMC inflammation panel, the following assays were selected from the Life Tech Taqman repository: HPRT1 (Taqman Mm01545399_m1), B2M (Taqman Mm00437762_m1), CD247 (Taqman Mm00446171_m1), EMR1 (Taqman Mm00802529_m1), ICAM-1 (Taqman Mm00516023_m1), IFN- β 1 (Taqman Mm00439552_s1), IL-12 α (Taqman Mm00434165_m1), IL15 (Taqman Mm00434210_m1), IL1 β (Taqman Mm00434228_m1), IL6 (Taqman Mm00446190_m1), CCL2 (Taqman Mm00441242_m1), TNF α (Taqman Mm00443258_m1), Ms4a1 (Taqman Mm00545909_m1), and VCAM (Taqman Mm01320970_m1). The -fold changes in expression were calculated by using the average $\Delta\Delta C_t$ for the gene of interest in the C57BL/10 group as reference. Statistical analysis consisted of a two-way ANOVA followed by a Tukey's multicomparison test performed on the $\Delta\Delta C_t$ values.

Statistical analysis

Where appropriate, statistical significance was calculated using either Student's *t*-test or two-way ANOVA tests for independent samples with post hoc Bonferroni comparisons for each possible pair of groups, unless otherwise noted. Calculations were performed using Prism v5 software (GraphPad Software). Any significant differences ($p < 0.05$) between the two control strains are denoted with the # symbol. Significant differences ($p < 0.05$) between the C57BL/10 and the B10-*mdx* strains are denoted with a black * symbol. Any significant differences ($p < 0.05$) between the DBA/2 and D2-*mdx* strains are denoted with a gray * symbol (symbol colors correspond to the coat colors for the two background strains).

Acknowledgements

We thank Debbie McClellan for the excellent editorial help.

Funding

Dr. Nagaraju is supported by National Institutes of Health (5U54HD053177; K26OD011171, P50AR060836-01), Muscular Dystrophy Association, and US Department of Defense (W81XWH-05-1-0616, W81XWH-11-1-0782).

Drs. Cox, Nagaraju and Lutz are supported by US Department of Defense (W81XWH-11-1-0330).

Conflict of interest statement

Dr. Nagaraju is the president of Agada biosciences, a contract research organization involved in preclinical drug testing in neuromuscular disease models.

References

- 1 Hatzipetros, T., Bogdanik, L.P., Tassinari, V.R., Kidd, J.D., Moreno, A.J., Davis, C., Osborne, M., Austin, A., Vieira, F.G. and Lutz, C. (2014) C57BL/6J congenic Prp-TDP43A315T mice develop progressive neurodegeneration in the myenteric plexus of the colon without exhibiting key features of ALS. *Brain research*, **1584**, 59-72.
- 2 Gallagher, M.D., Suh, E., Grossman, M., Elman, L., McCluskey, L., Van Swieten, J.C., Al-Sarraj, S., Neumann, M., Gelpi, E. and Ghetti, B. (2014) TMEM106B is a genetic modifier of frontotemporal lobar degeneration with C9orf72 hexanucleotide repeat expansions. *Acta neuropathologica*, **127**, 407-418.
- 3 Heiman-Patterson, T.D., Sher, R.B., Blankenhorn, E.A., Alexander, G., Deitch, J.S., Kunst, C.B., Maragakis, N. and Cox, G. (2011) Effect of genetic background on phenotype variability in transgenic mouse models of amyotrophic lateral sclerosis: a window of opportunity in the search for genetic modifiers. *Amyotrophic Lateral Sclerosis*, **12**, 79-86.
- 4 Heydemann, A., Ceco, E., Lim, J.E., Hadhazy, M., Ryder, P., Moran, J.L., Beier, D.R., Palmer, A.A. and McNally, E.M. (2009) Latent TGF- β -binding protein 4 modifies muscular dystrophy in mice. *The Journal of clinical investigation*, **119**, 3703.
- 5 Sicinski, P., Geng, Y., Ryder-Cook, A.S., Barnard, E.A., Darlison, M.G. and Barnard, P.J. (1989) The molecular basis of muscular dystrophy in the mdx mouse: a point mutation. *Science*, **244**, 1578-1580.
- 6 Ryder-Cook, A., Sicinski, P., Thomas, K., Davies, K., Worton, R., Barnard, E., Darlison, M. and Barnard, P. (1988) Localization of the mdx mutation within the mouse dystrophin gene. *The EMBO journal*, **7**, 3017.
- 7 Chamberlain, J.S., Metzger, J., Reyes, M., Townsend, D. and Faulkner, J.A. (2007) Dystrophin-deficient mdx mice display a reduced life span and are susceptible to spontaneous rhabdomyosarcoma. *The FASEB Journal*, **21**, 2195-2204.
- 8 Stedman, H.H., Sweeney, H.L., Shrager, J.B., Maguire, H.C., Panettieri, R.A., Petrof, B., Narusawa, M., Leferovich, J.M., Sladky, J.T. and Kelly, A.M. (1991) The mdx mouse diaphragm reproduces the degenerative changes of Duchenne muscular dystrophy. *Nature*, **352**, 536-539.
- 9 Heydemann, A., Ceco, E., Lim, J.E., Hadhazy, M., Ryder, P., Moran, J.L., Beier, D.R., Palmer, A.A. and McNally, E.M. (2010) Latent TGF- β -binding protein 4 modifies muscular dystrophy in mice. *The Journal of clinical investigation*, **120**, 645.
- 10 Fukada, S.-i., Morikawa, D., Yamamoto, Y., Yoshida, T., Sumie, N., Yamaguchi, M., Ito, T., Miyagoe-Suzuki, Y., Takeda, S.i. and Tsujikawa, K. (2010) Genetic background affects

- properties of satellite cells and mdx phenotypes. *The American journal of pathology*, **176**, 2414-2424.
- 11 Kornegay, J.N., Childers, M.K., Bogan, D.J., Bogan, J.R., Nghiem, P., Wang, J., Fan, Z., Howard, J.F., Jr., Schatzberg, S.J., Dow, J.L. *et al.* (2012) The paradox of muscle hypertrophy in muscular dystrophy. *Physical medicine and rehabilitation clinics of North America*, **23**, 149-172, xii.
 - 12 Baudy, A.R., Sali, A., Jordan, S., Kesari, A., Johnston, H.K., Hoffman, E.P. and Nagaraju, K. (2011) Non-invasive optical imaging of muscle pathology in mdx mice using cathepsin caged near-infrared imaging. *Mol Imaging Biol*, **13**, 462-470.
 - 13 Saad, A.D., Obinata, T. and Fischman, D.A. (1987) Immunochemical analysis of protein isoforms in thick myofilaments of regenerating skeletal muscle. *Developmental biology*, **119**, 336-349.
 - 14 Selsby, J.T., Morine, K.J., Pendrak, K., Barton, E.R. and Sweeney, H.L. (2012) Rescue of dystrophic skeletal muscle by PGC-1alpha involves a fast to slow fiber type shift in the mdx mouse. *PLoS one*, **7**, e30063.
 - 15 Roma, J., Munell, F., Fargas, A. and Roig, M. (2004) Evolution of pathological changes in the gastrocnemius of the mdx mice correlate with utrophin and β -dystroglycan expression. *Acta neuropathologica*, **108**, 443-452.
 - 16 Haslett, J.N., Sanoudou, D., Kho, A.T., Bennett, R.R., Greenberg, S.A., Kohane, I.S., Beggs, A.H. and Kunkel, L.M. (2002) Gene expression comparison of biopsies from Duchenne muscular dystrophy (DMD) and normal skeletal muscle. *Proceedings of the National Academy of Sciences*, **99**, 15000-15005.
 - 17 Montagutelli, X. (2000) Effect of the genetic background on the phenotype of mouse mutations. *Journal of the American Society of Nephrology*, **11**, S101-S105.
 - 18 Duddy, W., Duguez, S., Johnston, H., Cohen, T.V., Phadke, A., Gordish-Dressman, H., Nagaraju, K., Gnocchi, V., Low, S. and Partridge, T. (2015) Muscular dystrophy in the mdx mouse is a severe myopathy compounded by hypotrophy, hypertrophy and hyperplasia. *Skeletal muscle*, **5**, 1-18.
 - 19 Lynch, G.S., Hinkle, R.T., Chamberlain, J.S., Brooks, S.V. and Faulkner, J.A. (2001) Force and power output of fast and slow skeletal muscles from mdx mice 6-28 months old. *The Journal of physiology*, **535**, 591-600.
 - 20 Takeda, A., Jimi, T., Wakayama, Y., Misugi, N., Miyake, S. and Kumagai, T. (1992) Demonstration of cathepsins B, H and L in xenografts of normal and Duchenne-muscular-dystrophy muscles transplanted into nude mice. *The Biochemical journal*, **288** (Pt 2), 643-648.
 - 21 Chen, Y.W., Nagaraju, K., Bakay, M., McIntyre, O., Rawat, R., Shi, R. and Hoffman, E.P. (2005) Early onset of inflammation and later involvement of TGFbeta in Duchenne muscular dystrophy. *Neurology*, **65**, 826-834.
 - 22 Spurney, C.F., Gordish-Dressman, H., Guerron, A.D., Sali, A., Pandey, G.S., Rawat, R., Van Der Meulen, J.H., Cha, H.J., Pistilli, E.E., Partridge, T.A. *et al.* (2009) Preclinical drug trials in the mdx mouse: assessment of reliable and sensitive outcome measures. *Muscle Nerve*, **39**, 591-602.
 - 23 Flanigan, K.M., Ceko, E., Lamar, K.M., Kaminoh, Y., Dunn, D.M., Mendell, J.R., King, W.M., Pestronk, A., Florence, J.M., Mathews, K.D. *et al.* (2013) LTBP4 genotype predicts age of ambulatory loss in Duchenne muscular dystrophy. *Annals of neurology*, **73**, 481-488.
 - 24 Van den Broek, F. and Beynen, A. (1998) The influence of dietary phosphorus and magnesium concentrations on the calcium content of heart and kidneys of DBA/2 and NMRI mice. *Laboratory Animals*, **32**, 483-491.
 - 25 Spurney, C.F., Knobloch, S., Pistilli, E.E., Nagaraju, K., Martin, G.R. and Hoffman, E.P. (2008) Dystrophin-deficient cardiomyopathy in mouse: Expression of Nox4 and Lox are associated with fibrosis and altered functional parameters in the heart. *Neuromuscul Disord*, **18**, 371-381.

Figure Legends

FIGURE 1: Loss of body mass in the D2.MDX strain was observed independently. Body mass was recorded for all four strains independently at both CNMC (A) and The Jackson Laboratory (B). Results for body weights taken at 28 weeks are shown. Significant differences within the same genetic background are marked with the (*) symbol. Significant differences between the two MDX strains are marked with the (#) symbol. B10.MDX mice were heavier than their B10 wild type controls as expected. In contrast, the D2.MDX strain was consistently smaller than DBA2 control

FIGURE 2: D2.MDX mice do not exhibit hypertrophy as is seen in B10.MDX mice. The tibialis anterior from each mouse was dissected at 12 weeks and preserved in 4% formalin prior to staining for reticulin (A). Fiber diameter was then measured for each strain as shown in (B). The histograms in the center show all of the available data, while the flanking histograms provide a zoomed-in look at the extreme ends of the full data set. The distribution of fiber diameters in B10.MDX mice was found to be skewed toward larger fibers compared to the control C57Bl10 strain, consistent with fiber hypertrophy. In contrast, the D2.MDX mice were found to possess smaller fiber diameters than their DBA2 controls. Small diameter fibers can result from branched or atrophic muscle fibers.

FIGURE 3: Both MDX strains show similar serum CK profiles. Levels of CK enzyme activity in the serum from all four strains were measured at 28 weeks at CNMC (A) and at 24 weeks at The Jackson Laboratory (B). The results were consistent between the two labs. Serum CK levels for D2.MDX mice were significantly higher than normal baseline levels, but on average were lower than levels seen in B10.MDX mice.

FIGURE 4: D2.MDX show and increased levels of Evans Blue Dye uptake compared B10.MDX. In order to quantify muscle fiber damage, the gastrocnemius and tibialis anterior (TA) muscle were dissected from all four strains of mice at 8 weeks of age. All mice were injected with EBD 24 hours prior to being sacrificed. Representative fluorescent cross sections from B10.MDX (A,B) and D2.MDX (C,D) muscles show retained EBD in red and positive myh3 staining in green. EBD content from gastrocnemius lysates was quantified by spectroscopy (E).

FIGURE 5: Loss of grip strength in the D2.MDX strain was observed independently. Forelimb grip strength was recorded for all four strains independently at both CNMC (A) and The Jackson Laboratory (B). Results for grip strength taken at 28 weeks are shown. All grip strength measurements are normalized to the individual animal's body weight. Both MDX strains were significantly weaker than their wild type controls. The same trends in forelimb grip strength were also reproducible between labs.

FIGURE 6: D2.MDX mice experience significant muscle weakness at all ages. Force contraction analysis was performed on the freshly dissected EDL muscle of all strains at 7, 28, and 52 weeks at CNMC. Data for the mass of the EDL muscle (A), maximum force generation (B), and specific force generation (C) are shown. The B10.MDX mice showed the expected deficit in specific force generation starting at 28 weeks. However, D2.MDX mice displayed significant muscle weakness both in terms of maximum and specific force generation beginning at the earliest time point. The mass EDL of the D2.MDX mouse was also significantly lower than its wild type control.

FIGURE 7: D2.MDX mice develop signs of cardiomyopathy earlier than B10.MDX mice. Echocardiography was performed by CNMC at 7, 28 and 52 weeks (A,B) for each mouse strain. The data analysis showed that the D2.MDX mice showed detectable deficits in the ejection fraction (A) and shortening fraction (B) starting at 28 weeks, prior to the appearance of any cardiomyopathy in B10.MDX mice. The functional deficits in cardiac function were corroborated by histological results.

FIGURE 8A: Both MDX strains show inflammation in the diaphragm at all ages. The diaphragm from each mouse was dissected at 7, 28, and 52 weeks and preserved in 4% formalin prior to H&E staining. Tissue histology was normal for the control C57Bl10 and DBA2 strains. The B10.MDX strain showed expected inflammation in the diaphragm. The D2.MDX strain displayed inflammation and calcifications (see indicated examples) in the diaphragm at 7 weeks of age. Calcium deposits were only observed in the diaphragm of D2.MDX mice.

FIGURE 8B: D2.MDX mice show signs of cardiomyopathy at 7 weeks of age. The heart from each mouse was dissected at 7, 28, and 52 weeks and preserved in 4% formalin prior to H&E staining. Tissue histology was normal for the control C57Bl10 and DBA2 strains. All images show transverse sections of the left ventricle wall. The B10.MDX did not show signs of cardiomyopathy until 28 weeks. The D2.MDX strain displayed inflammation and calcifications (see indicated examples) in the heart starting at 7 weeks of age. Calcium deposits were only observed in the D2.MDX mice.

FIGURE 9: *In vivo* optical imaging confirms increased cathepsin activity and inflammation in MDX strains. The cathepsin-mediated cleavage of the ProSense 680 dye serves as a quantifiable marker for inflammation *in vivo*. Sedated mice were imaged at 7 weeks and 52 weeks of age at CNMC. Cathepsin activity was measured in the fore limbs (A) and in the hind limbs (B). Cathepsin activity was significantly higher in both MDX strains at 7 weeks of age when compared to their respective healthy control strains.

FIGURE 10: D2.MDX mice display significant differences in inflammatory gene expression. We isolated mRNA from frozen TA muscle tissue from 6 week and 52 week old animals to examine inflammatory gene expression via QRT-PCR. A selection of significantly altered genes are shown in panels A-F. C57Bl10 mice at 52 weeks were used as a baseline for all calculations of changes in relative gene expression. Both D2.MDX and B10.MDX mice showed the same trends in the expression over time for both soluble cytokines (A-E) and

macrophage surface markers (F). Note that the changes in expression in D2.MDX mice are greater in magnitude than in the B10.MDX mice.

FIGURE 11: D2.MDX mice show a deficiency of central nuclei despite nuclear proliferation in damaged tissues and similar expression of . Central nuclei are used as markers for successful muscle fiber regeneration. The tibialis anterior of BRDU-treated animals and prepared for either H&E staining (A,B) or immunofluorescence (C,D). Frozen sections were stained with anti-BRDU (green colored) and anti-laminin (red colored). The proportion of centrally-nucleated fibers versus healthy uninjured fibers was quantified for all four strains (E). Both MDX mutant strains possessed significantly more central nucleated fibers than their respective controls. The quantification of BRDU-labeled nuclei showed that both strains had similar numbers of newly proliferated cells (F) but that the D2.MDX mice possessed fewer BRDU⁺ central nuclei than B10.MDX mice. Myosin gene expression in the TA was determined for all four strains by QRT-PCR (H). The D2.MDX mice suffered from greater muscle fiber damage than B10.MDX mice as measured by EBD uptake. However, levels of embryonic myosin (myh3) or perinatal myosin (myh8) were comparable between the two MDX strains.

Supplemental Figure Legends

Supplemental Figure 1. Both MDX strains have weaker grip strengths than their respective control strains. Fore limb and hind limb grip strength were measured by CNMC at 28 and 52 weeks (A&B). Fore limb grip strength was also measured by The Jackson Lab (C) at 6, 12 and 24 weeks for all mouse strains. All grip strength measurements are normalized to the animal's bodyweight. The two sets of results are consistent. The B10.MDX animals are significantly weaker at all time points. The D2.MDX mice are weaker compared to the DBA2 controls starting at 12 weeks, but the gap between healthy DBA2 and diseased D2.MDX animals appears to close over time.

Supplemental Figure 2. D2.MDX mice develop signs of cardiomyopathy earlier than B10.MDX mice. Echocardiography was performed by CNMC at 7, 28 and 52 weeks for each mouse strain. The data analysis showed that the D2.MDX mice showed detectable deficits starting at 28 weeks in left ventricular volume (A) and cardiac output (B) but not in the B10.MDX mice.

Supplemental Figure 3. Both MDX strains show inflammation in the quadriceps at all ages. The heart from each mouse was dissected at 7, 28, and 52 weeks and preserved in 4% formalin prior to H&E staining. Tissue histology was normal for the control C57Bl10 and DBA2 strains. Both mutant MDX strains showed signs of inflammation and mononuclear cell infiltration at all time points. Calcium deposits were not observed in the B10.MDX mice until 52 weeks. The D2.MDX strain displayed inflammation and calcifications as early as 7 weeks.

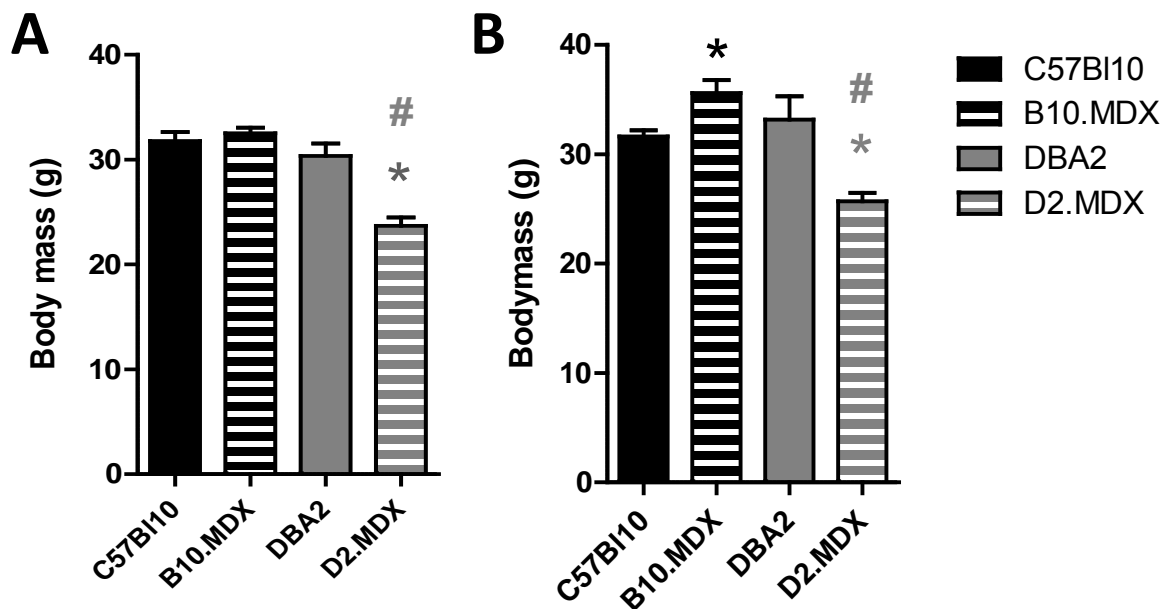
Supplemental Figure 4. Calcium deposition significantly alters tissue density in D2.MDX mice. The quadriceps, heart, and diaphragm from each mouse was dissected at 7 weeks and preserved in 4% formalin. Preserved tissues were then imaged using a MicroCT scan to a

resolution of 9 μm by CNMC. Example 3D reconstruction images of the quadriceps (A), hearts (B), and diaphragm (C) are shown in subpanels, showing the calcification in heart are mainly in the epicardium near apex. Tissue densities were calculated from 3D-images for the quadriceps (D), heart (E) and diaphragm (F) for all strains (n=3). Tissue densities for the D2.MDX mice were significantly higher in all examined muscle tissues.

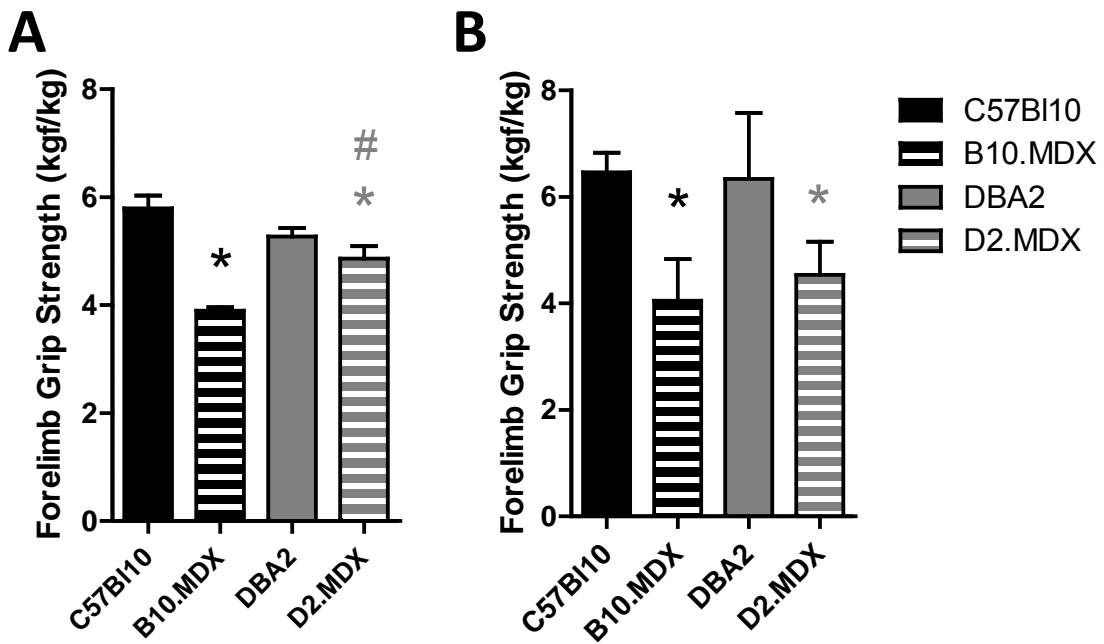
Supplemental Figure 5. *In vivo* optical imaging confirms increased cathepsin activity and inflammation in MDX strains. The cathepsin-mediated cleavage of the ProSense 680 dye serves as a quantifiable marker for inflammation *in vivo*. Sedated mice were imaged at 7 weeks and 52 weeks of age at CNMC. Cathepsin activity was measured in the fore limbs and in the hind limbs. Representative images from DBA2, D2.MDX, BL10 and B10.MDX mice at 7 weeks and 52 weeks are shown. Signal from the limbs was gated as shown. Cathepsin activity is false colored by a heat map gradient, where red indicates high cumulative activity and purple indicates low activity.

Abbreviations

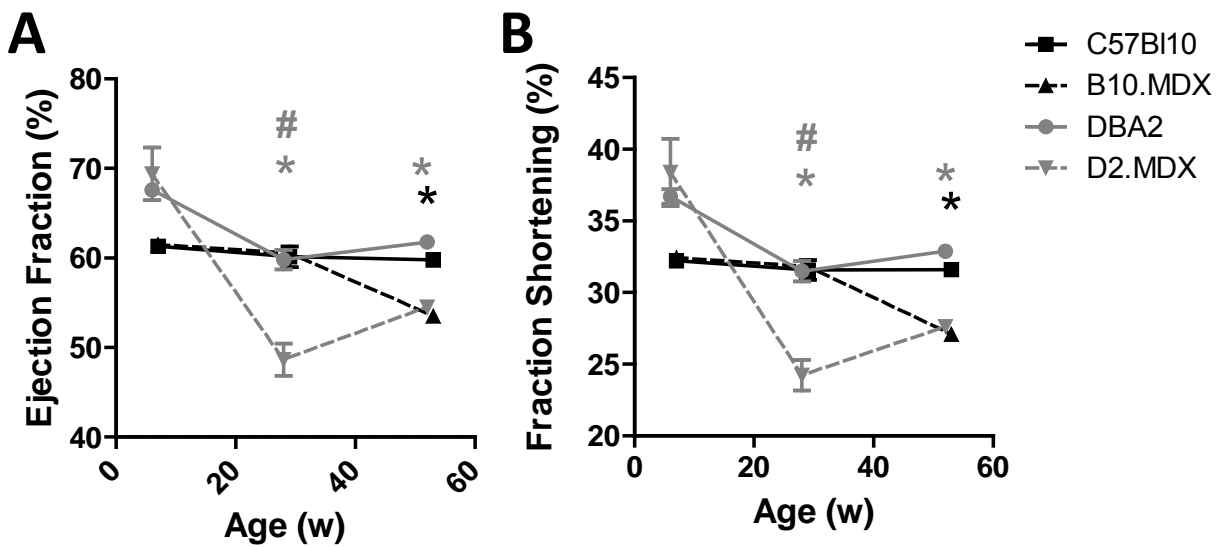
BRDU: bromodeoxyuridine
CK: creatine kinase
CNF: central nucleated fibers
CTSB: cathepsin B
DMD: Duchenne muscular dystrophy
Dmd: dystrophin gene
EBD: evan blue dye
EDL: extensor digitorum longus
GSM: grip strength measurement
LV: left ventricle
mRNA: messenger RNA
TA: tibialis anterior
TGF- β : transforming growth factor beta



Loss of body mass in the D2.MDX strain was observed independently. Body mass was recorded for all four strains independently at both CNMC (A) and The Jackson Laboratory (B). Results for body weights taken at 28 weeks are shown. Significant differences within the same genetic background are marked with the (*) symbol. Significant differences between the two MDX strains are marked with the (#) symbol. B110.MDX mice were heavier than their B110 wild type controls as expected. In contrast, the D2.MDX strain was consistently smaller than DBA2 control

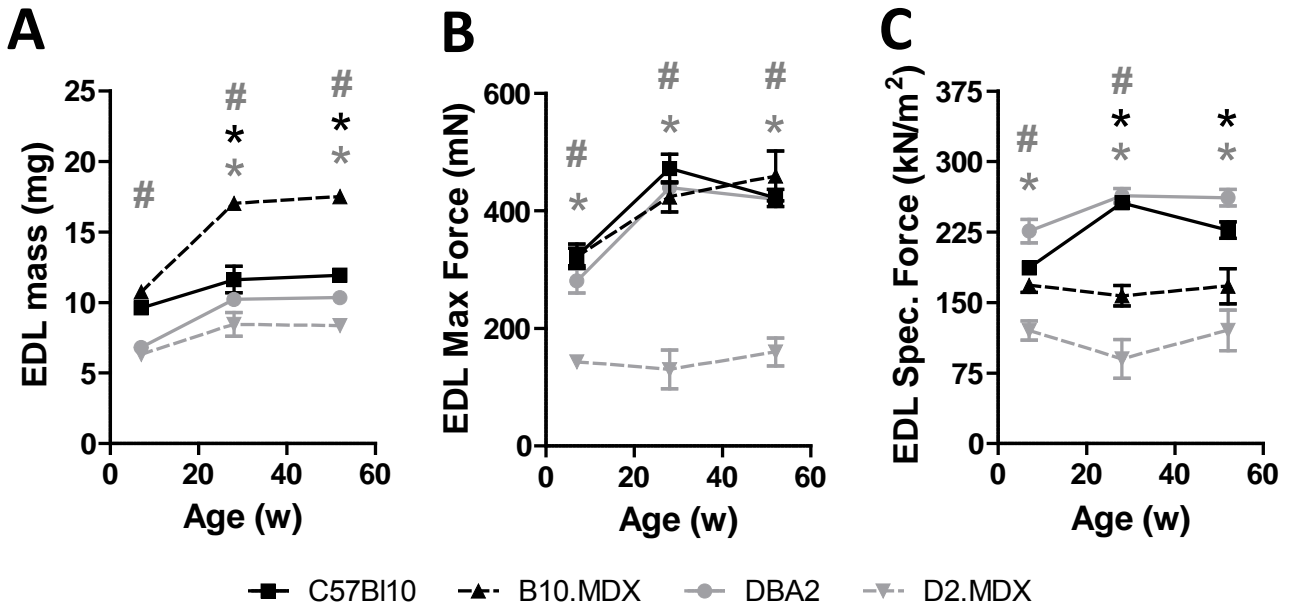


Loss of grip strength in the D2.MDX strain was observed independently. Forelimb grip strength was recorded for all four strains independently at both CNMC (A) and The Jackson Laboratory (B). Results for grip strength taken at 28 weeks are shown. All grip strength measurements are normalized to the individual animal's body weight. Both MDX strains were significantly weaker than their wild type controls. The same trends in forelimb grip strength were also reproducible between labs.

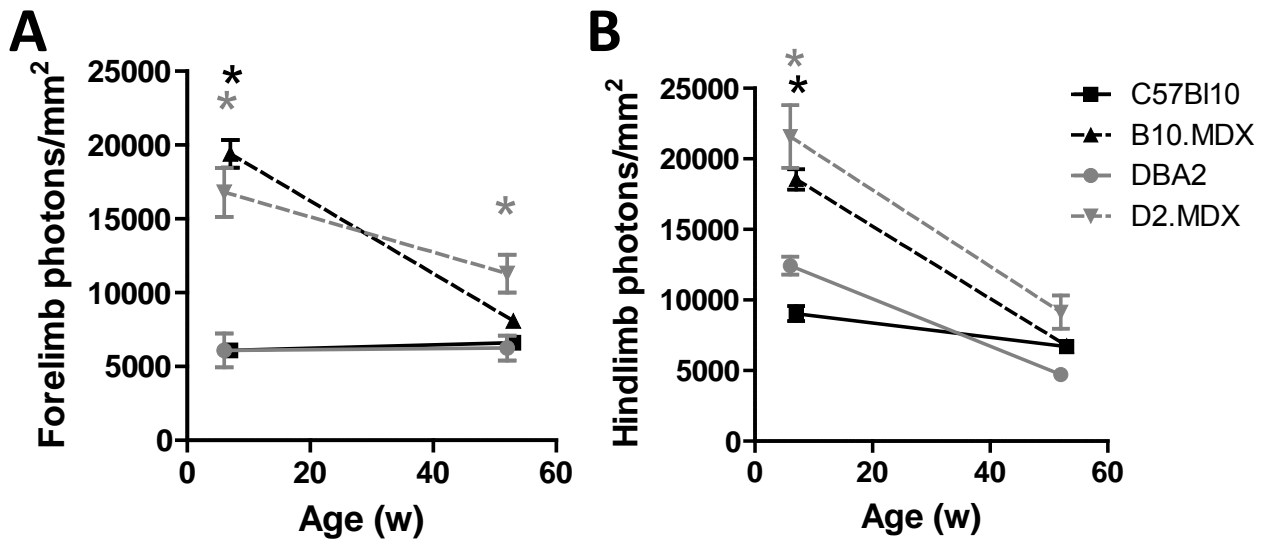


D2.MDX mice develop signs of cardiomyopathy earlier than B10.MDX mice.

Echocardiography was performed by CNMC at 7, 28 and 52 weeks (A,B) for each mouse strain. The data analysis showed that the D2.MDX mice showed detectable deficits in the ejection fraction (A) and shortening fraction (B) starting at 28 weeks, prior to the appearance of any cardiomyopathy in B10.MDX mice. The functional deficits in cardiac function were corroborated by histological results.

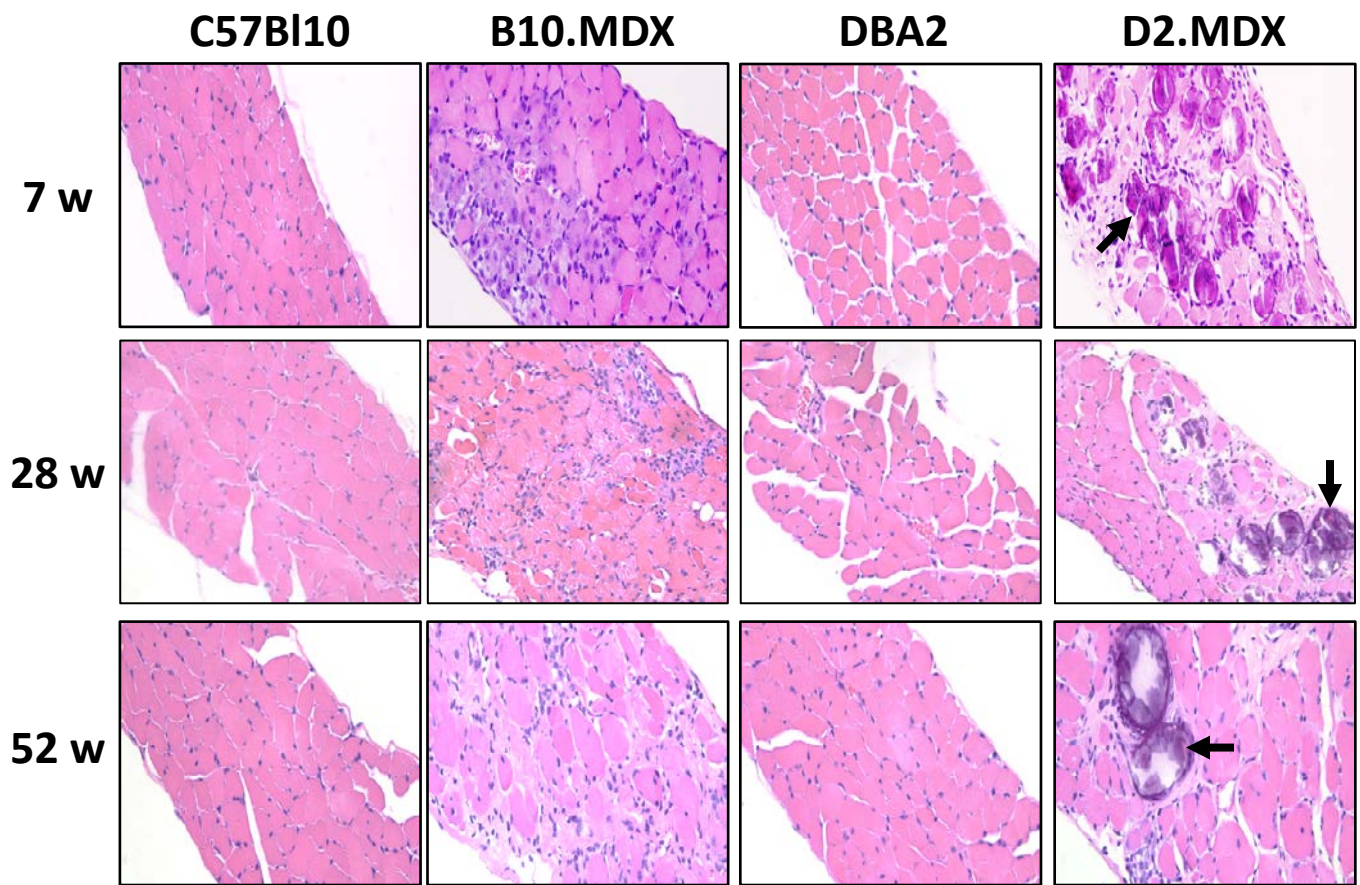


D2.MDX mice experience significant muscle weakness at all ages. Force contraction analysis was performed on the freshly dissected EDL muscle of all strains at 7, 28, and 52 weeks at CNMC. Data for the maximum force generation (A), specific force generation (B), and mass of the EDL muscle (C) are shown. The B10.MDX mice showed the expected deficit in specific force generation starting at 28 weeks. However, D2.MDX mice displayed significant muscle weakness both in terms of maximum and specific force generation beginning at the earliest time point. The mass EDL of the D2.MDX mouse was also significantly lower than its wild type control.

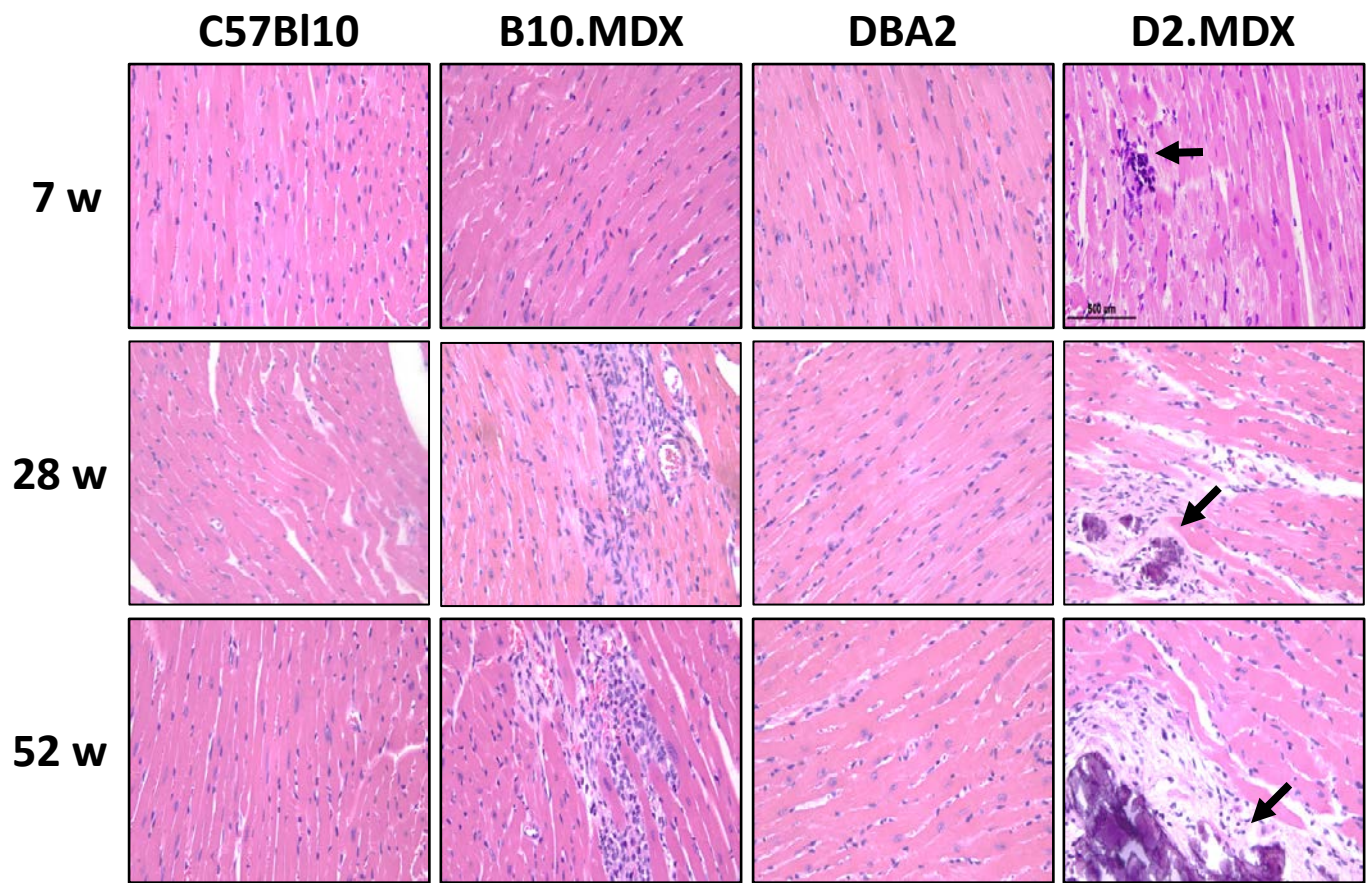


***In vivo* optical imaging confirms increased cathepsin activity and inflammation in MDX strains.**

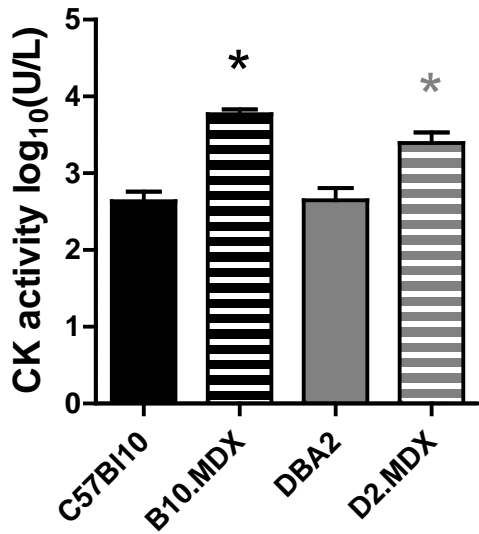
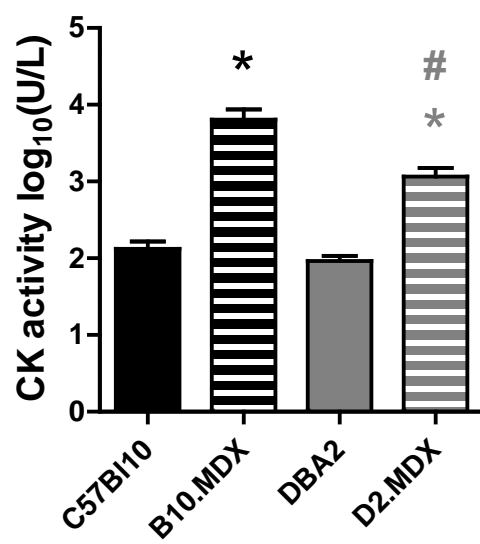
The cathepsin-mediated cleavage of the ProSense 680 dye serves as a quantifiable marker for inflammation *in vivo*. Sedated mice were imaged at 7 weeks and 52 weeks of age at CNMC. Cathepsin activity was measured in the fore limbs (A) and in the hind limbs (B). Cathepsin activity was significantly higher in both MDX strains at 7 weeks of age when compared to their respective healthy control strains.



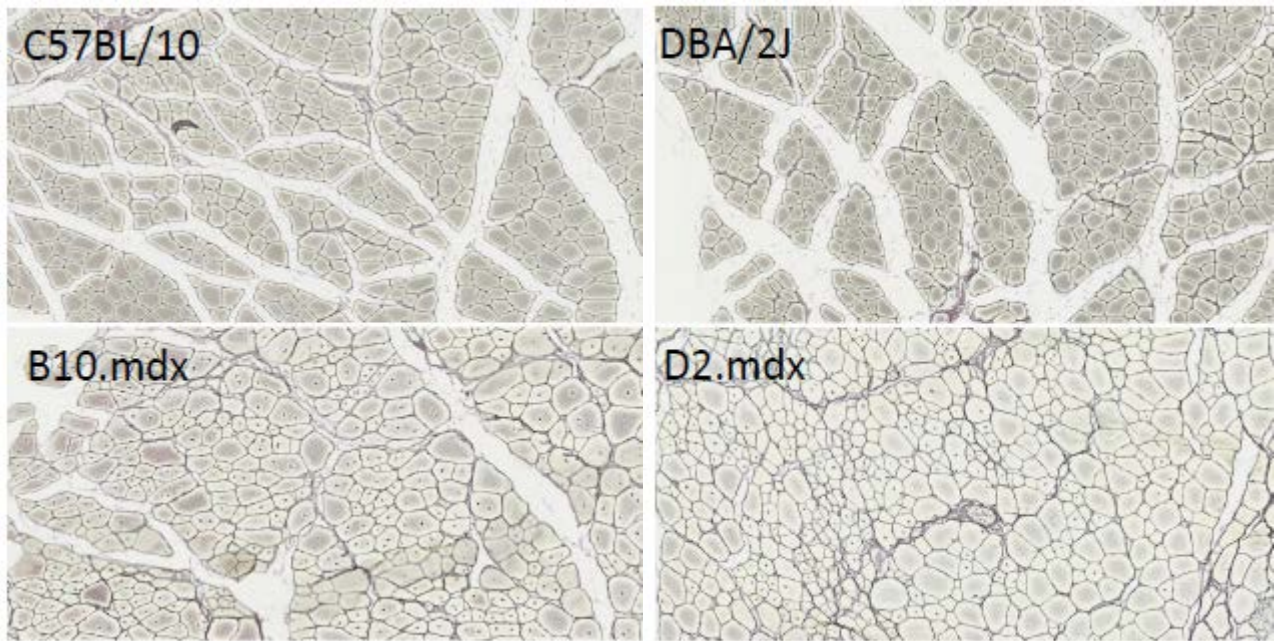
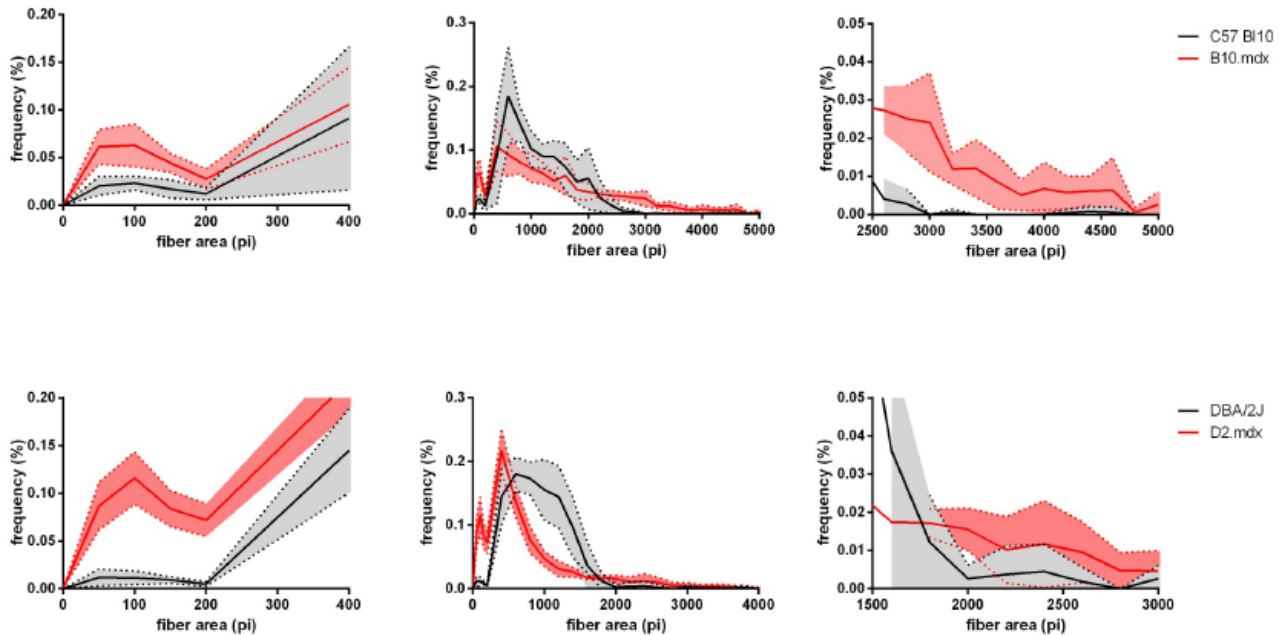
Both MDX strains show inflammation in the diaphragm at all ages. The diaphragm from each mouse was dissected at 7, 28, and 52 weeks and preserved in 4% formalin prior to H&E staining. Tissue histology was normal for the control C57Bl10 and DBA2 strains. The B10.MDX strain showed expected inflammation in the diaphragm. The D2.MDX strain displayed inflammation and calcifications (see indicated examples) in the diaphragm at 7 weeks of age. Calcium deposits were only observed in the diaphragm of D2.MDX mice.



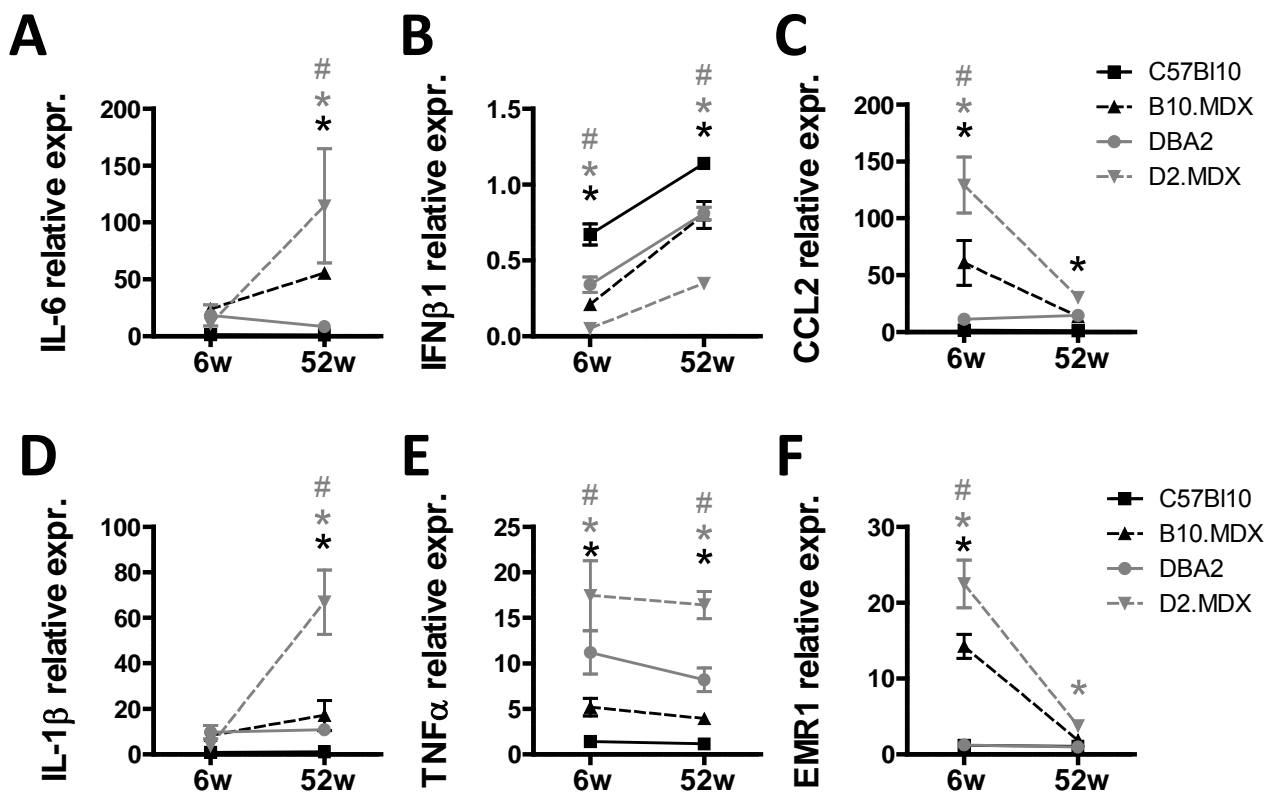
D2.MDX mice show signs of cardiomyopathy at 7 weeks of age. The heart from each mouse was dissected at 7,28, and 52 weeks and preserved in 4% formalin prior to H&E staining. Tissue histology was normal for the control C57Bl10 and DBA2 strains. All images show transverse sections of the left ventricle wall. The B10.MDX did not show signs of cardiomyopathy until 28 weeks. The D2.MDX strain displayed inflammation and calcifications (see indicated examples) in the heart starting at 7 weeks of age. Calcium deposits were only observed in the D2.MDX mice.

A**B**

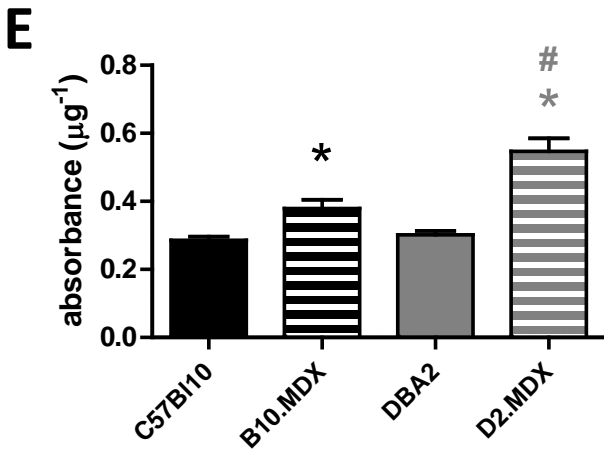
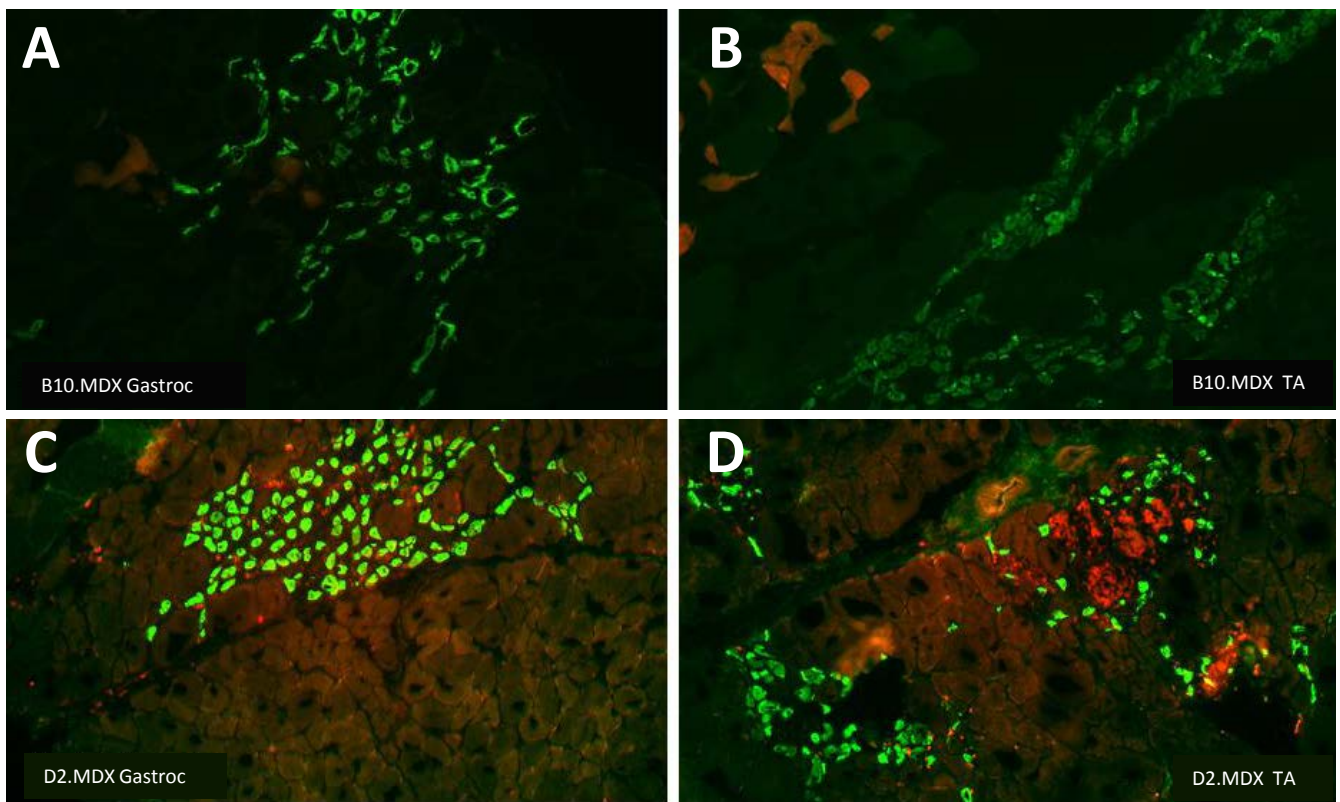
Both MDX strains show similar serum CK profiles. Levels of CK enzyme activity in the serum from all four strains were measured at 28 weeks at CNMC (A) and at 24 weeks at The Jackson Laboratory (B). The results were consistent between the two labs. Serum CK levels for D2.MDX mice were significantly higher than normal baseline levels, but on average were lower than levels seen in B10.MDX mice.

A**B**

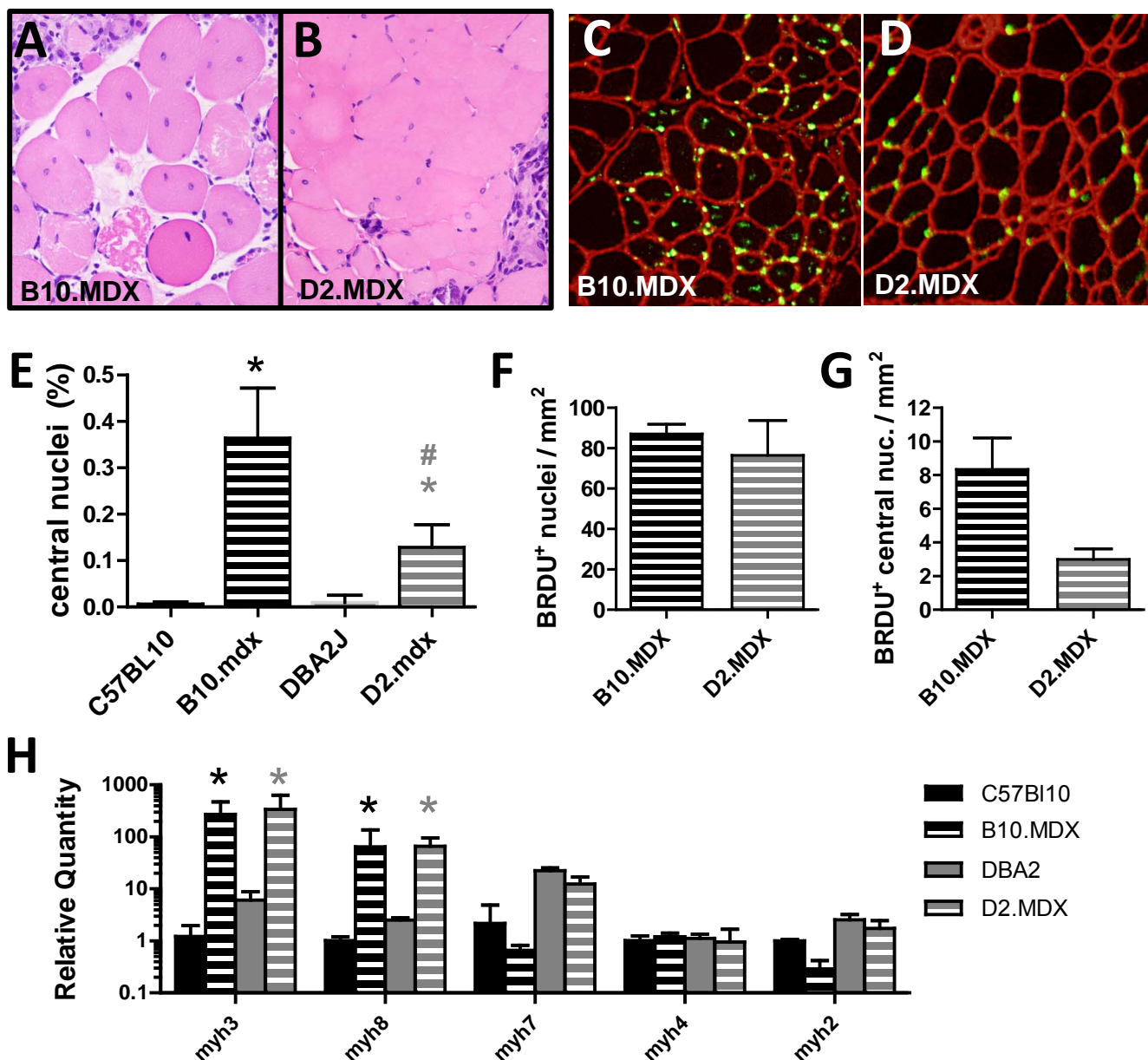
D2.MDX mice do not exhibit hypertrophy as is seen in B10.MDX mice. The tibialis anterior from each mouse was dissected at 12 weeks and preserved in 4% formalin prior to staining for reticulin (A). Fiber diameter was then measured for each strain as shown in (B). The histograms in the center show all of the available data, while the flanking histograms provide a zoomed-in look at the extreme ends of the full data set. The distribution of fiber diameters in B10.MDX mice was found to be skewed toward larger fibers compared to the control C57BL/10 strain, consistent with fiber hypertrophy. In contrast, the D2.MDX mice were found to possess smaller fiber diameters than their DBA/2J controls. Small diameter fibers can result from branched or atrophic muscle fibers.



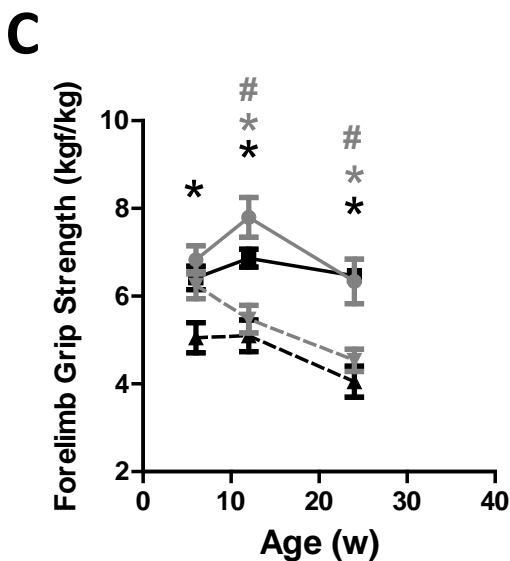
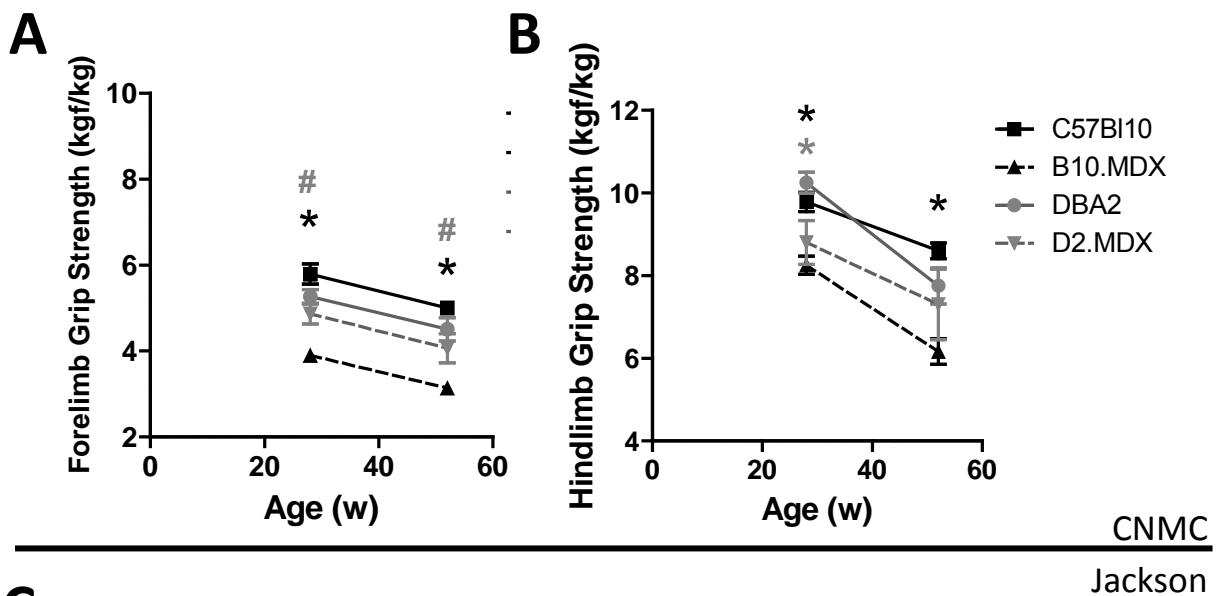
D2.MDX mice display significant differences in inflammatory gene expression. We isolated mRNA from frozen TA muscle tissue from 6 week and 52 week old animals to examine inflammatory gene expression via QRT-PCR. A selection of significantly altered genes are shown in panels A-F. C57Bl10 mice at 52 weeks were used as a baseline for all calculations of changes in relative gene expression. Both D2.MDX and B10.MDX mice showed the same trends in the expression over time for both soluble cytokines (A-E) and macrophage surface markers (F). Note that the changes in expression in D2.MDX mice are greater in magnitude than in the B10.MDX mice.



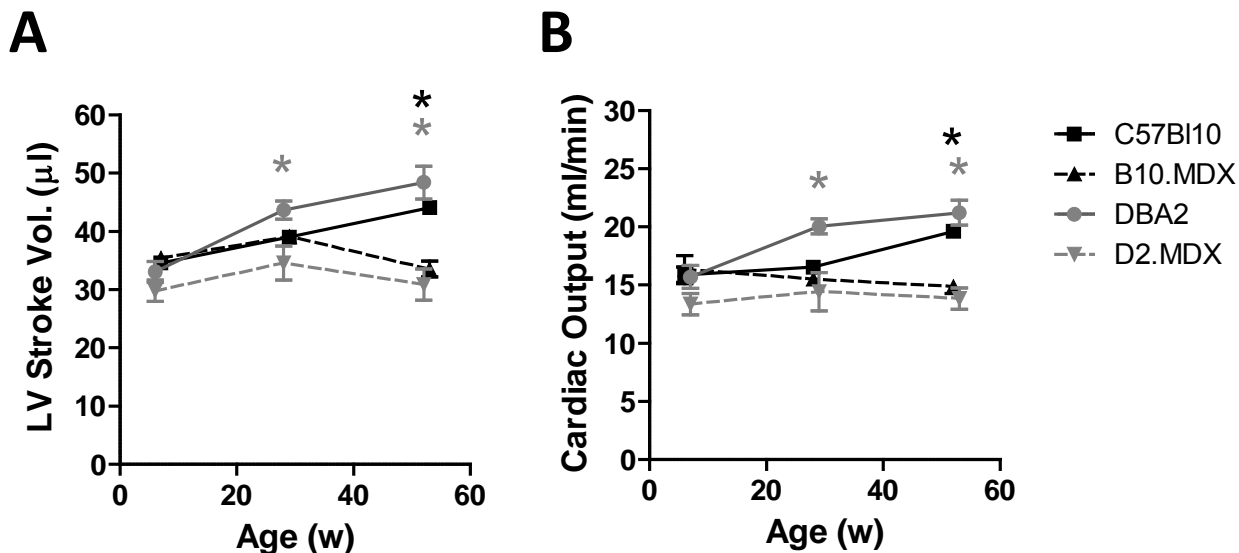
D2.MDX show and increased levels of Evans Blue Dye uptake compared B10.MDX. In order to quantify muscle fiber damage, the gastrocnemius and tibialis anterior (TA) muscle were dissected from all four strains of mice at 8 weeks of age. All mice were injected with EBD 24 hours prior to being sacrificed. Representative fluorescent cross sections from B10.MDX (A,B) and D2.MDX (C,D) muscles show retained EBD in red and positive myh3 staining in green. EBD content from gastrocnemius lysates was quantified by spectroscopy (E).



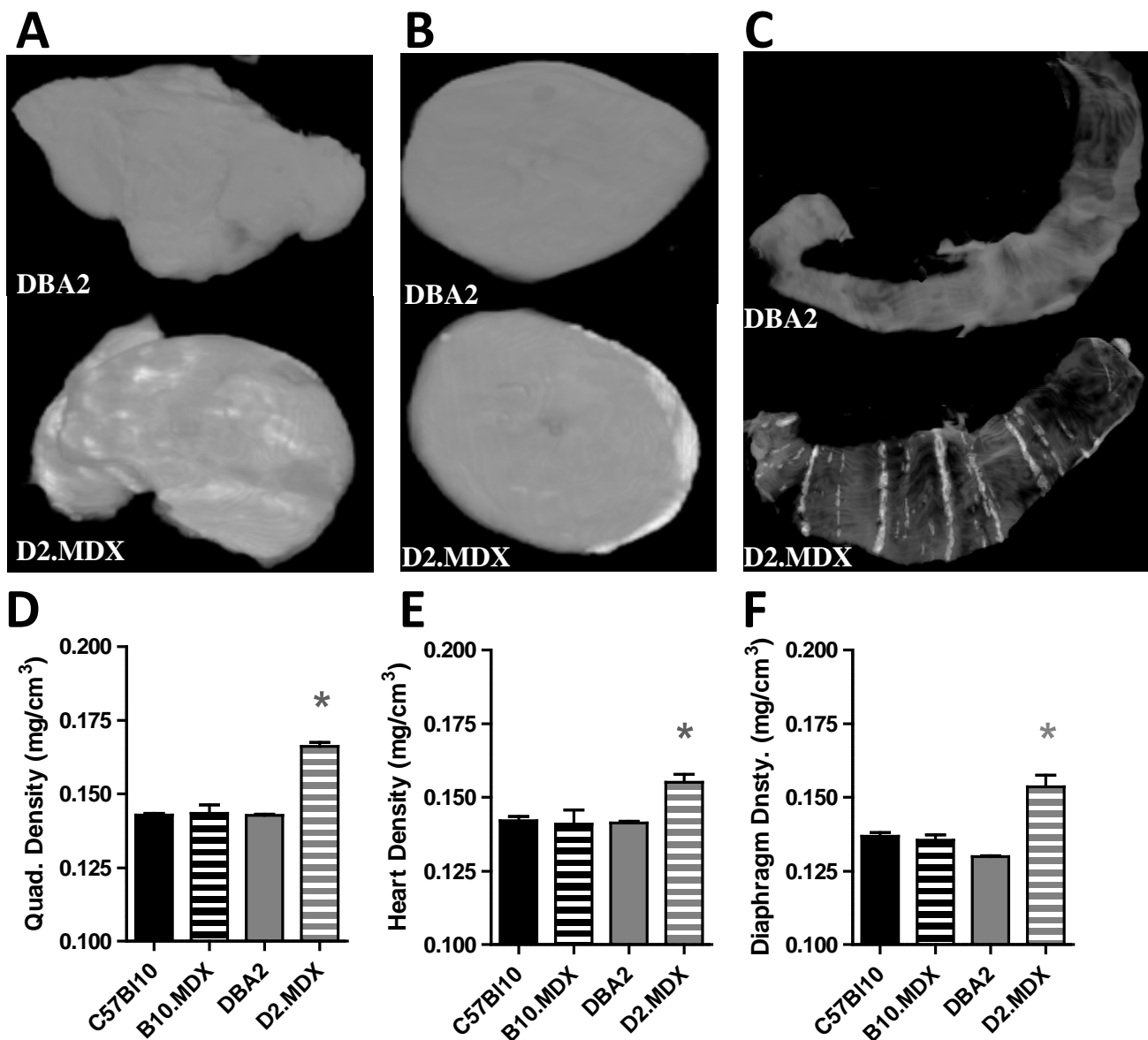
D2.MDX mice show a deficiency of central nuclei despite nuclear proliferation in damaged tissues and similar expression of . Central nuclei are used as markers for successful muscle fiber regeneration. The tibialis anterior of BRDU-treated animals and prepared for either H&E staining (A,B) or immunofluorescence (C,D). Frozen sections were stained with anti-BRDU (green colored) and anti-laminin (red colored). The proportion of centrally-nucleated fibers versus healthy uninjured fibers was quantified for all four strains (E). Both MDX mutant strains possessed significantly more central nucleated fibers than their respective controls. The quantification of BRDU-labeled nuclei showed that both strains had similar numbers of newly proliferated cells (F) but that the D2.MDX mice possessed fewer BRDU⁺ central nuclei than B10.MDX mice. Myosin gene expression in the TA was determined for all four strains by QRT-PCR (H). The D2.MDX mice suffered from greater muscle fiber damage than B10.MDX mice as measured by EBD uptake. However, levels of embryonic myosin (myh3) or perinatal myosin (myh8) were comparable between the two MDX strains.



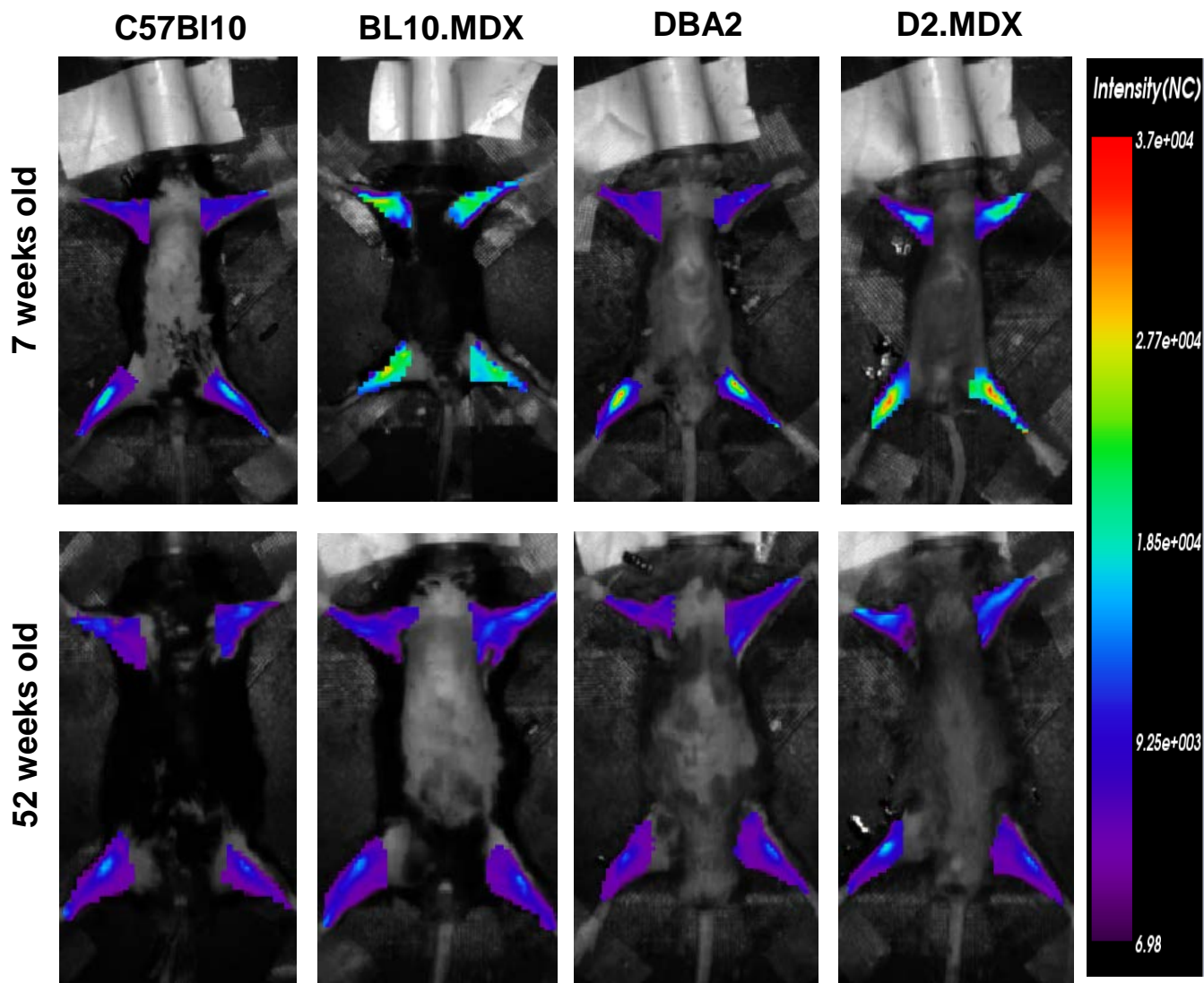
Supplemental Figure. Both MDX strains have weaker grip strengths than their respective control strains. Fore limb and hind limb grip strength were measured by CNMC at 28 and 52 weeks (*A&B*). Fore limb grip strength was also measured by The Jackson Lab (*C*) at 6, 12 and 24 weeks for all mouse strains. All grip strength measurements are normalized to the animal's bodyweight. The two sets of results are consistent. The B10.MDX animals are significantly weaker at all time points. The D2.MDX mice are weaker compared to the DBA2 controls starting at 12 weeks, but the gap between healthy DBA2 and diseased D2.MDX animals appears to close over time.



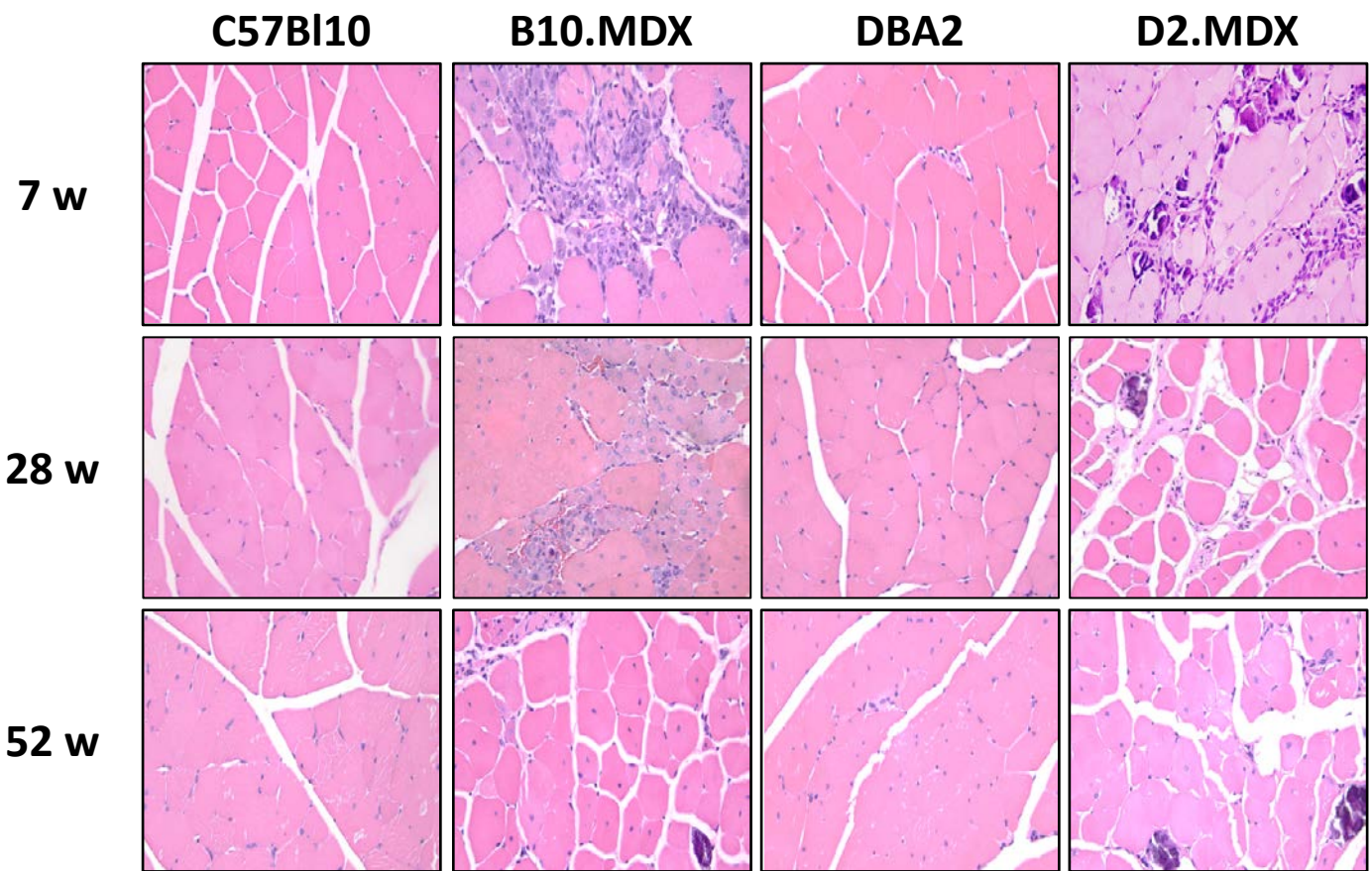
Supplemental Figure. D2.MDX mice develop signs of cardiomyopathy earlier than B10.MDX mice. Echocardiography was performed by CNMC at 7, 28 and 52 weeks for each mouse strain. The data analysis showed that the D2.MDX mice showed detectable deficits starting at 28 weeks in left ventricular volume (A) and cardiac output (B) but not in the B10.MDX mice.



Supplemental Figure. Calcium deposition significantly alters tissue density in D2.MDX mice. The quadriceps, heart, and diaphragm from each mouse was dissected at 7 weeks and preserved in 4% formalin. Preserved tissues were then imaged using a MicroCT scan to a resolution of 9 μm by CNMC. Example 3D reconstruction images of the quadriceps (A), hearts (B), and diaphragm (C) are shown in subpanels, showing the calcification in heart are mainly in the epicardium near apex. Tissue densities were calculated from 3D-images for the quadriceps (D), heart (E) and diaphragm (F) for all strains (n=3). Tissue densities for the D2.MDX mice were significantly higher in all examined muscle tissues.



Supplemental Figure. *In vivo* optical imaging confirms increased cathepsin activity and inflammation in MDX strains. The cathepsin-mediated cleavage of the ProSense 680 dye serves as a quantifiable marker for inflammation *in vivo*. Sedated mice were imaged at 7 weeks and 52 weeks of age at CNMC. Cathepsin activity was measured in the fore limbs and in the hind limbs. Representative images from DBA2, D2.MDX, BL10 and B110.MDX mice at 7 weeks and 52 weeks are shown. Signal from the limbs was gated as shown. Cathepsin activity is false colored by a heat map gradient, where red indicates high cumulative activity and purple indicates low activity.



Supplemental Figure. Both MDX strains show inflammation in the quadriceps at all ages. The heart from each mouse was dissected at 7,28, and 52 weeks and preserved in 4% formalin prior to H&E staining. Tissue histology was normal for the control C57Bl10 and DBA2 strains. Both mutant MDX strains showed signs of inflammation and mononuclear cell infiltration at all time points. Calcium deposits were not observed in the B10.MDX mice until 52 weeks. The D2.MDX strain displayed inflammation and calcifications as early as 7 weeks.

Sup. Table: Inflammatory surface markers and cytokine expression at 7 weeks.

	C57Bl10 7w	DBA2 7w	B10.MDX 7w	D2.MDX 7w
CD247 (CD3z)	-1.03	-5.15	-2.13	-3.77
Ms4a1 (CD20)	-1.44	-1.32	-4.09	-2.63
EMR1 (F4/80)	1.19	1.25	14.25	22.48
B2M	-1.06	-1.17	-1.18	1.89
VCAM	-1.10	1.35	2.13	2.29
ICAM-1	-1.04	1.45	1.98	3.09
IL1 β	-1.25	9.76	8.28	3.77
IL-6	1.36	18.26	23.90	10.77
CCL2	1.58	11.31	60.95	129.33
TNF α	1.39	11.21	5.19	17.46
IFN- β 1	-1.49	-2.91	-4.78	-19.18
IL-12	-1.07	3.12	-1.08	1.99
IL-15	-1.20	-1.32	-2.20	-3.88

Sup. Table: Inflammatory surface markers and cytokine expression at 12 weeks.

	C57Bl10 12w	DBA2 12w	B10.MDX 12w	D2.MDX 12w
CD53	1.09	1.04	6.91	27.55
CD48	1.10	0.83	5.97	16.81
LTB	1.07	1.74	3.47	31.95
CD11b	1.07	0.99	9.89	45.69
Lgals3	1.19	1.22	24.95	77.36
Ly6c1	1.06	1.56	1.63	5.27
Mpeg1	1.24	1.06	25.82	86.33
TNF α	1.19	8.80	4.41	23.24
IL-6	1.36	1.99	1.97	9.37
C1qB	1.10	0.95	9.39	9.89

Sup. Table: Inflammatory surface markers and cytokine expression at 52 weeks.

	C57Bl10 52w	DBA2 52w	B10.MDX 52w	D2.MDX 52w
CD247 (CD3z)	1.11	1.04	-2.24	1.05
Ms4a1 (CD20)	1.12	-13.23	-2.03	-7.04
EMR1 (F4/80)	1.09	-1.03	1.85	3.76
B2M	1.09	1.10	1.55	3.45
VCAM	1.13	-2.24	-4.18	-1.31
ICAM-1	1.01	-1.31	-1.50	1.39
IL1 β	1.13	10.85	17.13	66.92
IL-6	1.14	8.53	55.54	114.60
CCL2	1.13	14.47	13.69	30.54
TNF α	1.14	8.21	3.93	16.42
IFN- β 1	1.14	-1.23	-1.25	-2.87
IL-12	1.05	1.70	1.36	3.36
IL-15	-1.04	-1.85	-1.67	-1.22

Supplementary Table 1: Average body mass and tissue weights

	C57Bl10	B10.MDX	DBA2	D2.MDX
(g)	BodyMass	BodyMass	BodyMass	BodyMass
7 w	21.17 ±0.49	24.77 ±0.4	19.72 ±1.09	18.13 ±0.96
28 w	35.41 ±1.36	32.52 ±0.54	30.37 ±0.76	23.68 ±0.81
52 w	34.55 ±0.81	33.82 ±0.98	32.14 ±1.36	26.35 ±1.45
	C57Bl10	B10.MDX	DBA2	D2.MDX
(mg)	EDL Mass	EDL Mass	EDL Mass	EDL Mass
7 w	9.61 ±0.34	10.74 ±0.41	6.83 ±0.32	6.32 ±0.25
28 w	11.63 ±0.94	17.04 ±0.41	10.22 ±0.24	8.44 ±0.83
52 w	11.94 ±0.4	17.51 ±0.48	10.35 ±0.32	8.38 ±0.48
	C57Bl10	B10.MDX	DBA2	D2.MDX
(mg)	Soleus Mass	Soleus Mass	Soleus Mass	Soleus Mass
7 w	5.85 ±0.44	7.98 ±0.34	5.04 ±0.49	4.69 ±0.25
28 w	11.23 ±0.90	12.17 ±0.64	6.45 ±0.32	7.08 ±0.28
52 w	9.9 ±0.54	13.84 ±0.5	6.9 ±0.33	7.18 ±0.35
	C57Bl10	B10.MDX	DBA2	D2.MDX
(mg)	Gastroc mass	Gastroc mass	Gastroc mass	Gastroc mass
7 w	106.28 ±2.78	122.49 ±2.83	75.81 ±4.39	68.93 ±3.20
28 w	136.67 ±7.83	177.77 ±7.34	108.92 ±2.83	64.48 ±2.57
52 w	163.81 ±4.78	138.5 ±2.72	108.45 ±3.21	49.93 ±2.27
	C57Bl10	B10.MDX	DBA2	D2.MDX
(mg)	TA mass	TA mass	TA mass	TA mass
7 w	32.43 ±1.46	50.67 ±1.87	26.76 ±2.06	24.34 ±0.98
28 w	48.78 ±3.15	64.14 ±1.75	39.00 ±1.41	27.96 ±1.50
52 w	42.88 ±1.18	59.96 ±2.30	35.03 ±1.50	25.53 ±4.86
	C57Bl10	B10.MDX	DBA2	D2.MDX
(mg)	Quad Mass	Quad Mass	Quad Mass	Quad Mass
7 w	145.78 ±12.07	192.66 ±8.08	123.40 ±8.48	94.49 ±5.21
28 w	N/A	314.58 ±6.83	164.69 ±4.83	106.58 ±4.22
52 w	209.23 ±5.76	276.60 ±7.53	170.37 ±4.22	82.58 ±6.12
	C57Bl10	B10.MDX	DBA2	D2.MDX
(mg)	Spleen Mass	Spleen Mass	Spleen Mass	Spleen Mass
7 w	88.30 ±3.31	150.32 ±8.13	72.33 ±4.12	81.46 ±5.08
28 w	76.93 ±7.53	125.58 ±5.39	89.97 ±5.79	81.04 ±4.24
52 w	90.17 ±3.8	105.18 ±6.26	92.68 ±6.73	82.10 ±6.13
	C57Bl10	B10.MDX	DBA2	D2.MDX
(mg)	Heart mass	Heart mass	Heart mass	Heart mass
7 w	107.28 ±2.88	110.14 ±4.97	111.00 ±6.75	111.05 ±4.97
28 w	118.00 ±8.3	155.27 ±5.03	179.39 ±3.54	167.38 ±8.94
52 w	148.01 ±5.45	165.22 ±5.35	208.27 ±6.49	210.80 ±14.24

Supplementary Table 2: Average ratio of tissue mass to matching body mass

	C57Bl10	B10.MDX	DBA2	D2.MDX
(mg/g)	EDL % of BM	EDL % of BM	EDL % of BM	EDL % of BM
7 w	0.45 ±0.01	0.43 ±0.01	0.35 ±0.01	0.35 ±0.02
28 w	0.33 ±0.03	0.52 ±0.01	0.34 ±0.01	0.36 ±0.03
52 w	0.35 ±0.01	0.52 ±0.01	0.33 ±0.01	0.32 ±0.01
	C57Bl10	B10.MDX	DBA2	D2.MDX
(mg/g)	Soleus % of BM	Soleus % of BM	Soleus % of BM	Soleus % of BM
7 w	0.28 ±0.02	0.32 ±0.01	0.26 ±0.02	0.26 ±0.02
28 w	0.32 ±0.01	0.37 ±0.02	0.21 ±0.01	0.3 ±0.01
52 w	0.29 ±0.02	0.41 ±0.02	0.22 ±0.01	0.27 ±0.00
	C57Bl10	B10.MDX	DBA2	D2.MDX
(mg/g)	Gastroc % of BM	Gastroc % of BM	Gastroc % of BM	Gastroc % of BM
7 w	5.02 ±0.07	4.95 ±0.09	3.84 ±0.05	3.83 ±0.12
28 w	3.86 ±0.13	5.45 ±0.15	3.6 ±0.10	2.73 ±0.13
52 w	4.77 ±0.25	4.11 ±0.14	3.4 ±0.08	1.9 ±0.06
	C57Bl10	B10.MDX	DBA2	D2.MDX
(mg/g)	TA % of BM	TA % of BM	TA % of BM	TA % of BM
7 w	1.53 ±0.05	2.05 ±0.08	1.37 ±0.09	1.35 ±0.03
28 w	1.38 ±0.04	1.97 ±0.04	1.29 ±0.06	1.19 ±0.07
52 w	1.24 ±0.06	1.78 ±0.09	1.1 ±0.05	0.95 ±0.13
	C57Bl10	B10.MDX	DBA2	D2.MDX
(mg/g)	Quad % of BM	Quad % of BM	Quad % of BM	Quad % of BM
7 w	6.91 ±0.58	6.97 ±0.92	6.22 ±0.14	4.04 ±0.91
28 w	N/A	9.68 ±0.17	5.43 ±0.09	4.54 ±0.31
52 w	6.06 ±0.28	8.19 ±0.21	5.36 ±0.15	3.13 ±0.10
	C57Bl10	B10.MDX	DBA2	D2.MDX
(mg/g)	Spleen % of BM	Spleen % of BM	Spleen % of BM	Spleen % of BM
7 w	4.17 ±0.13	6.07 ±0.32	3.68 ±0.16	4.52 ±0.23
28 w	2.17 ±0.20	3.86 ±0.15	3.00 ±0.21	3.42 ±0.14
52 w	2.35 ±0.31	3.12 ±0.21	2.90 ±0.19	3.14 ±0.29
	C57Bl10	B10.MDX	DBA2	D2.MDX
(mg/g)	Heart % of BM	Heart % of BM	Heart % of BM	Heart % of BM
7 w	5.07 ±0.09	4.45 ±0.18	5.63 ±0.12	6.16 ±0.16
28 w	3.34 ±0.23	4.77 ±0.12	5.94 ±0.15	7.08 ±0.39
52 w	4.33 ±0.24	4.91 ±0.27	6.53 ±0.15	7.98 ±0.10